Fabrication of 3-D Nanoscale Structures of Arbitrary Shape by a Single-step E-beam Grayscale Lithographic Process

by

Dong Liu

A thesis submitted to the Graduate Faculty of
Auburn University
in partial fulfillment of the
requirements for the Degree of
Master of Science

Auburn, Alabama
May 14, 2010

Keywords: electron beam lithography, 3-D structure,
reactive ion etching, grayscale, arbitrary shape

Approved by

Bart C. Prorok, Chair, Associate Professor of Materials Engineering
Dong-Joo Kim, Associate Professor of Materials Engineering
Soo-Young Lee, Professor of Electrical and Computer Engineering

Abstract

Three dimensional (3-D) structures are widely utilized and critical to device functionality in many applications, such as PBG (photonic band gap) crystals, DOE's (diffractive optical elements), blazed gratings, MEMS, NEMS etc. The performance characteristics of such structures are highly sensitive to their dimensional fidelity, which is strongly influenced by the fabrication process. In most cases, the fabricated structures were of microscale and regular shapes and their applications were therefore prohibited accordingly. In this study, grayscale electron beam lithography and reactive ion etching were employed to fabricate complex 3-D structures. With the aid of a unique algorithm, PYRAMID which aims at correcting proximity effect of EBL, three arbitrary shape 3-D structures were successfully fabricated on photoresist and Si substrate respectively. A series of major factors involved in fabrication process, dose coefficient, base dose, spot size, line spacing, developing time, developer concentration and ultrasonic agitation were studied one by one along with fabrication results. Design of Experiment was used to statistically determine the significance of individual factor and the cross effect of multiple factors and perform an optimization and prediction based upon existed experimental results. It is revealed that base dose, developing time, developer concentration and their interactions are significant factors in terms of as-fabricated structure geometry and resolution. A response optimization based upon experimental results were performed and 20 solutions were found consequently. Compare these solutions with the experimental factors used to achieve optimum response, it is concluded that the optimized solutions agree with experimental data.

Acknowledgements

I would like to thank my academic supervisor, Dr. Bart C. Prorok, for his critical supervision and high standard requirement on everything. This work can not be accomplished without his strict instruction.

Thanks also go to my co-supervisor, Dr. Soo-young Lee, for his academic dedication to EBL pattern correction and useful discussion during the fabrication process.

I am very grateful to my parents and my girlfriend during my study in US for the last three years. Their endless patience, forgiveness, support and love are always the greatest inspiration to me no matter where I am and what I do.

Those who helped me on my research during my study in Auburn university are not forgotten. They are Shakib Morshed, Nicole Odum, Adam Anderson, Aimee Poda, Naved, Charles Ilis, Weng Shen, Kewei Zhang, Xiaoxia Huang, Bo Zhou.

Last but not the least, special thanks to Dr. Tony Overfelt's financial support, I would have not wound up myself tough in the last semester here due to the stipend cut under the terrible economic slump.

Table of Contents

List of Tables

List of Figures

List of Abbreviations

EBL	Electron Beam Lithography
E-beam	Electron Beam
GEBL	Grayscale Electron Beam Lithography
RMS	Root Mean Surface
DOE	Design of Experiment
RIE	Reactive Ion Etching
DRIE	Deep Reactive Ion Etching
FZP	Fresnel Zone Plate
MOSFET	Metal Oxide Semiconductor Field Effect Transistor
RF	Radio Frequency
LNA	Low Noise Amplifier
VCO	Voltage Controlled Oscillator
f_{sr}	Self Resonance Frequency
TDD	Transdermal Drug Delivery
TBE	Transdermal Blood Extraction
IC	Integrated Circuits
PDMS	Polydimethylsiloxane
NIL	NanoImprinting Lithography

DPN	Dip Pen Nanolithography
SPM	Scanning Probe Microscope
AFM	Atomic Force Microscope
MF	Multiply Factor
NPGS	Nanometer Pattern Generating System
MIBK	Methyisobutyl ketone
IPA	Isopropyl alcohol
DF	Dose Factor
SEM	Scanning Electron Microscope
1P4M	One-Poly-Four-Metal

Chapter 1 Introduction

There are numerous electronic devices that utilize 3-D structures of various shapes, such as arrays of particles [1, 2], gratings [3, 4], PBG (photonic band gap) crystal [5, 6], DOE (diffractive optical element) [7, 8], MRAM and NEMS (nanoelectromechanical systems) [9, 10] etc. The properties of these structures show high sensitivity to their dimensional measures like shape, size, etc., which often result in enhanced device functionality. As the feature size in these 3-D structures is decreased towards the nanoscale, it becomes more and more challenging to achieve high dimensional accuracy and reliability in their fabrication. Thus, there is a growing need for improving how accurately and reliably these 3-D structures are fabricated. In addition to man-made devices, numerous natural nanoscale objects exhibit well-controlled 3-D surfaces, on which the design of future revolutionary devices may be based. Hence, the ability of constructing 3-D nanoscale structures of arbitrary shape with high dimensional fidelity will not only contribute to efficient realization of the devices requiring such structures, but also trigger the development of never before conceived devices with new functionality.

Chapter 2 Literature review

2.1 Current application of 3-D micro/nano structures

2.1.1 Electronic devices

A 3-D gate structure incorporated into the 4H-SiC (0001) metal-oxide-semiconductor field-effect transistor(MOSFET) was fabricated by Japanese researchers[11]through plasma-enhanced chemical vapor deposition (PECVD) and reactive ion etching (RIE) to improve its electrical properties. This 3-D gate structure has a top channel on the (0001) face and side-wall channels on the (1120) face, whose schematic representations are

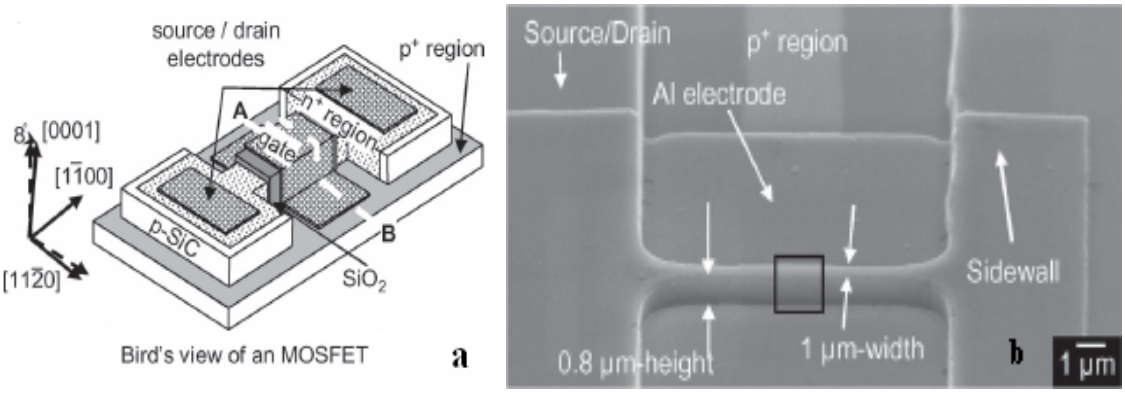

Figure 1. Schematic illustration a) Bird's eye view b) SEM of MOSFET with 3-D gate structure[11]

given in Figure 1. As a consequence, the fabricated MOSFET exhibited good characteristics on a series of electrical properties, such as the ION/IOFF ratio, the

subthreshold swing, and VTH are 10^9, 210 mV/decade, and 3.5 V respectively. Especially, the normalized drain current of a 1-um-wide MOSFET is 16 times than that of a conventional planar MOSFET.

On the other hand, complementary metal oxide semiconductor technology becomes an attractive candidate for low-gigahertz (<5 GHz) radio frequency (RF) applications with the continuing deduction of the gate length. However, the poor characteristics of the passive devices, especially the on-chip inductors and transformers, become the greatest obstacles to realize the fully integrated transceiver in CMOS technology. Usually, monolithic inductors are used in CMOS RF circuits, such as the low noise amplifier (LNA), voltage-controlled oscillator (VCO), and power amplifier. Unfortunately, the conventional spiral inductors implemented in the standard CMOS process suffer from poor quality factors due to the lossy property of the CMOS substrate and the thin metal layers. A novel miniature three dimensional structure inductor was proposed and fabricated in a standard digital 0.35- m one-poly-four-metal (1P4M) CMOS process to tackle this issue, as it is seen schematically in Figure 2. [12] As a result, the self-resonance frequency, f_{sr} of the proposed miniature 3-D inductor is 34% higher than the conventional stacked inductor.

Moreover, the proposed miniature 3-D inductor occupies only 16% of the area of the conventional planar spiral inductor with the same inductance and maximum quality factor max. By virtue of the small area of the miniature 3-D inductor, the size and cost of the radio frequency (RF) chip can be significantly reduced.

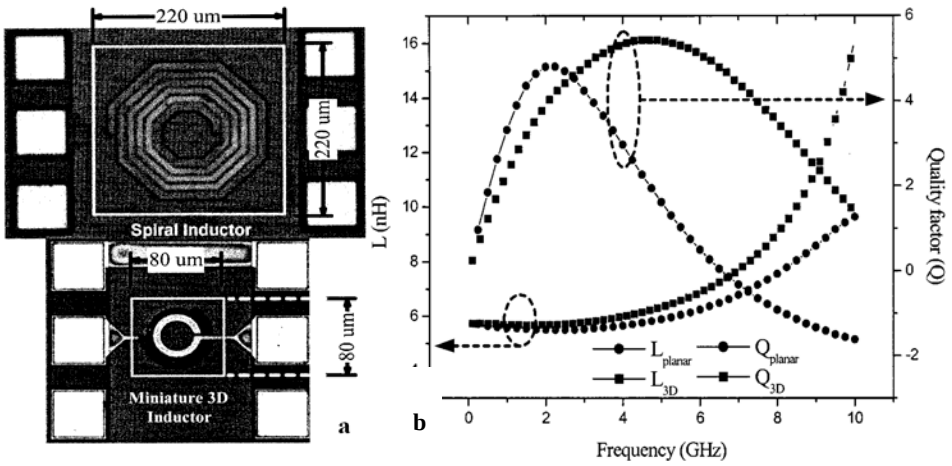

Figure 2. (a) Die photo of the planar inductor and a miniature 3-D inductor. (b) Measured inductances and quality factors of the planar and the miniature 3-D inductors[12]

2.1.2 Mechanical devices

Three dimensional structures also have widely applications in mechanical devices such as shown below. Figure 3 depicts a) 3-D structure nozzle plate and 3-D structure mold

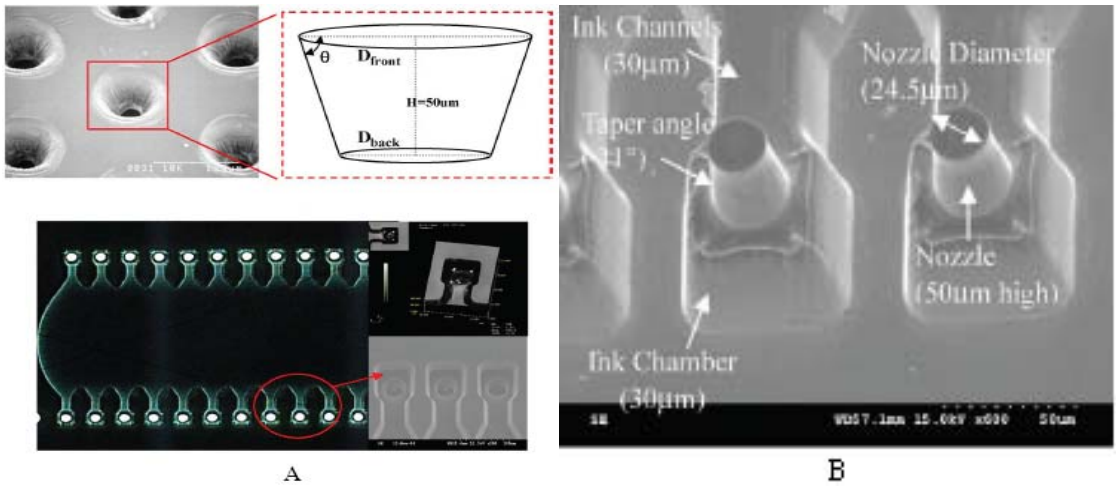

Figure 3. The picture of a 3-D structure A) nozzle plate and B) mold insert for a 1200 dpi inkjet printhead[13]

insert for a 1200 dots-per-inch (dpi) inkjet printhead. These interesting structures [13] were fabricated by an integration of excimer laser technology and microinjection molding, aiming at tackling the misalignment issue between the ink nozzle and ink chamber. It turns out that the operation cost can be reduced up to 50% along with a greatly improved print quality by using such the printhead packaged with such structure.

Wafer-level packaging is a powerful packaging approach for MEMS packaging which can meet the requirement of size, cost, and conditions such as vacuum. However, vacuum is a performance requirement for most of the MEMS devices. One of the criteria to have good vacuum reliability inside the package is to have a high degree of hermeticity because hermeticity is a measure of leakage of the gas flow from the package cavity.

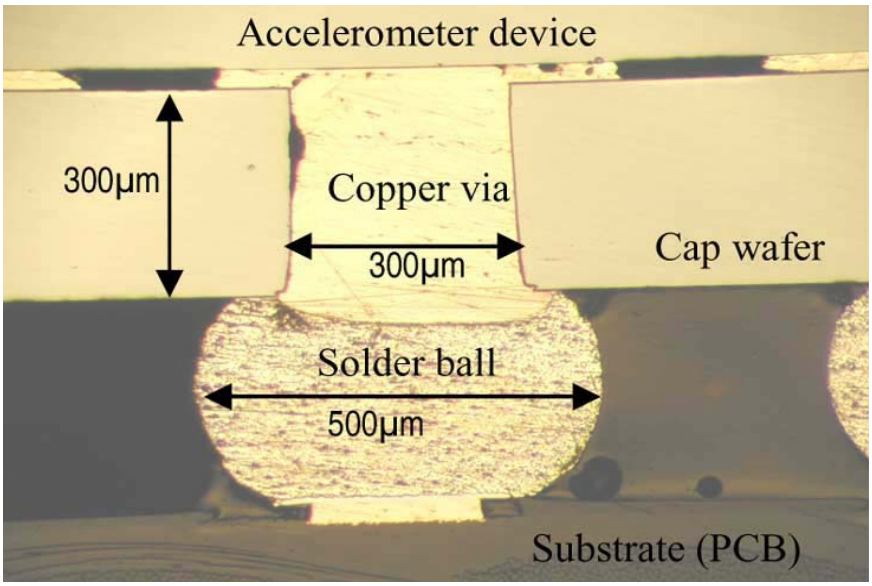

Figure 4. Cross-section of a 3-D wafer-level package of accelerometer device[14]

Figure 4 depicts a 3-D wafer-level vacuum package developed for an accelerometer device.[14] To maintain the vacuum inside the package wafer-level getter are deposited

and is activated during the wafer bonding process. The vacuum chamber formed by the accelerometer wafer and cap wafer was found to be 1 mtorr by indirect measurement of the Q-factor response of the accelerometer structure inside the package. Hermeticity and Current Voltage test showed no degradation in the device performance.

2.1.3 Optical devices

Astronomical telescope has been used by scientists to resolve the fine structure of an astronomical subject and separate multiple objects from each other in galaxy. The capability of a telescope depends on the angular resolution of itself. However, the angular resolution of current X-ray and gamma-ray telescopes have suffered from the difficulty in constructing concentrating optics due to the inherent nature of this high-energy radiation. Therefore, a Fresnel lens-based system, also called Fresnel Zone plate (FZP) for

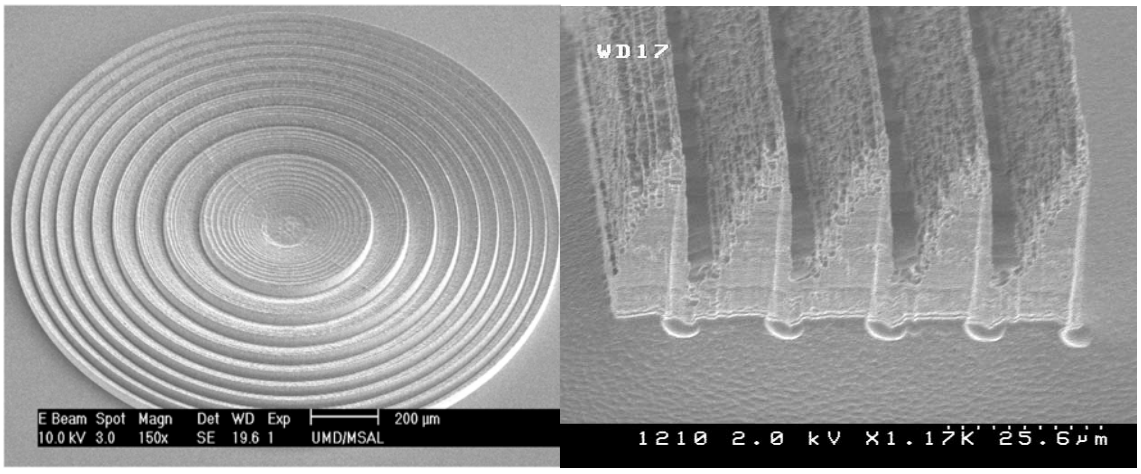

Figure 5. SEM graph of a Fresnel zone plate (FZP) consisted of 10 gratings (left side) and specific grating topography on FZP[15]

astronomical observations at hard X-ray and gamma-ray energies was proposed to tackle this issue. This system would have the highest diffraction-limited angular resolution of

any wavelength band, resulting in a greater than improvement over current gamma-ray imaging systems. The sensitivity of a Fresnel lens-based system would also be tremendous compared to typical background-limited gamma-ray instruments, resulting in an improvement. Most important, it has the potential to image previously unattainable events such as black hole event horizons, line emission from supernovae, and galactic microquasars. A typical FZP (left side) and its gratings (right side) fabricated by grayscale electron beam lithography and deep reactive ion etching (DRIE)[15] are shown in Figure 5.

Meanwhile, micro-optics fabrication appears to be a natural application due to the freedom in geometrical shape design, good optical properties of the photosensitive materials and rapid fabrication process which consists of very few steps, and already showed good results in micro-lens fabrication on a transparent substrate. Moreover, the realization of optical micro-structures has been reported in literature based on different techniques and appears to be of increasing interest for many applications. G. Cojoc etc [16] have fabricated a series of various 3-D structures with good optical properties on top of optical fibers by using the two-photon lithography (TPL) and their fabrications results are given below in figure 6. Various 3-D structures: a) convergent lens b) axicon lens c) ring shape phase mask are illustrated respectively in the left graph while in the right graph micro axicon lens with three apex angles a) 79º b) 117º c) 136º are given respectively. In terms of axicon lens, beam propagation from these structures shows a Bessel-like profile for a range of distance from the fiber end which is also dependent on

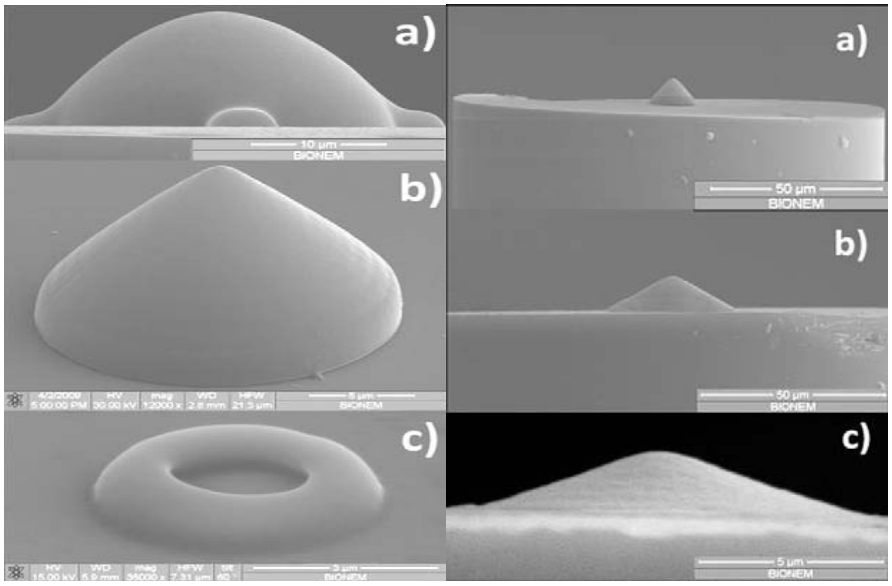

Figure 6. SEM illustration of various structures a) convergent lens b) axicon lens c) ring shape phase mask in the left graph and three axicon lens with a) 79° b) 119° c) 136° apex angle in the right graph, respectively[16]

the apex angle. In the vicinity of the conical lens, the full width of the central intensity peak is much smaller than the width of fiber fundamental mode: for the three apex angle, a full width down to around 0.75 um, 1.1 um and 1.22 um, respectively was obtained. This ability to create so small spots over relatively long distances, starting from the larger fiber mode, makes conical lenses on top of optical fibers interesting for many applications, e.g. near-field spectroscopy and optical coherence tomography.

2.1.4 Biological devices

Biologists also make use of 3-D structures to enhance their research. For example, in transdermal drug delivery (TDD) and transdermal blood extraction (TBE) applications, the conventional steel needle has been widely used. However, administration using the

conventional needle causes pain to patients while at the same time it is difficult to integrate this needle with other medical equipment such as small-scale point-of-care test devices. The microneedle overcomes these limitations because minimal invasive area reduces pain and its micro-scale structures can be integrated with other small devices. Researchers[17] found the deep x-ray a great candidate for high aspect ratio microneedle array fabrication, which consists of a vertical deep x-ray exposure and a successive inclined deep x-ray exposure. The first vertical exposure makes a triangular column array with a needle conduit through a deep x-ray mask having a triangular and hollow circle

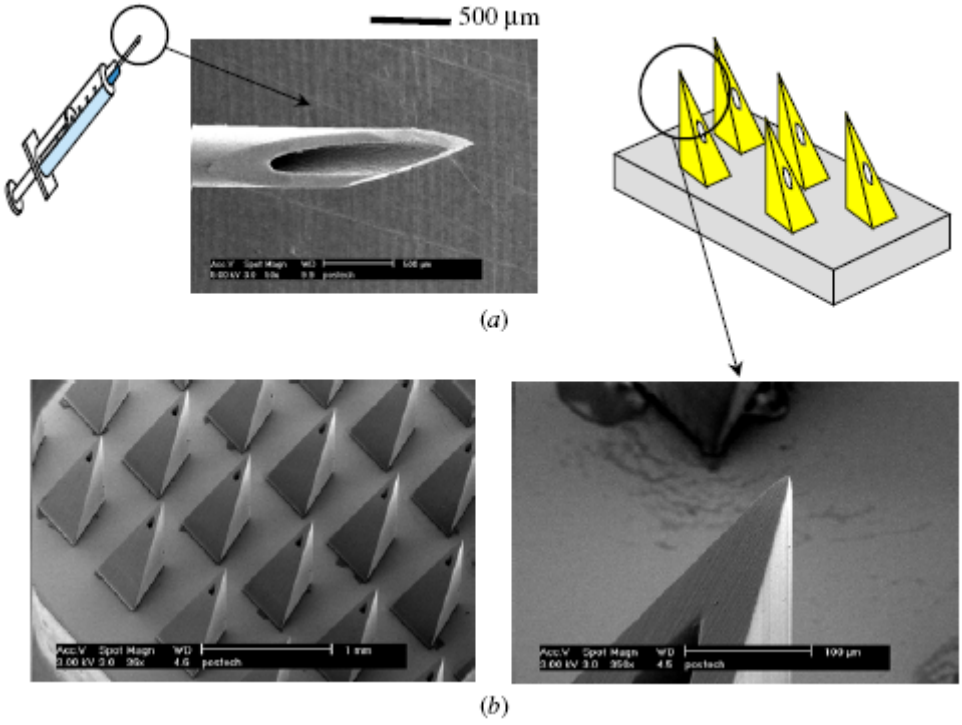

Figure 7. SEM images of the conventional stainless steel needle and fabricated microneedle array: (a) a conventional steel needle tip and (b) the fabricated PMMA microneedle array[17]

shape pattern. The column array is shaped into the microneedle array by the second inclined exposure without additional mask alignment. Changing the inclined angle and the gap between the mask and polymethylmethacrylate (positive photoresist) substrate, different types of microneedle arrays can be fabricated shown in figure 7.

2.2 Major techniques of fabricating 3-D micro/nanostructures

2.2.1 Lithography

Lithography makes a pattern in a resist on a substrate in order that the pattern can be duplicated sequentially on the substrate or other materials, which is added onto the substrate. A typical lithography process for integrated circuits (IC) fabrication involves exposing a resist to a beam of energetic particles, which are electrons, photons, or ions, by either passing a flood beam through a mask or scanning a focused beam. The particle beam changes the chemical structure of the exposed area of the resist layer. In subsequent etching, either the exposed area or the unexposed area of the resist will be removed to recreate the patterns. The resolution of a lithography method is limited by the wavelength of the particles, the particle scattering in the resist and the substrate, and the properties of the resist.

Several negative printing techniques are also available that rely on scanning probe instruments, electron beams, or molecular beams to pattern substrates using self-assembling monolayers and other organic materials as resist layers. Soft lithography includes near-field phase shift lithography, replica molding, micro-molding in capillaries, micro-transfer molding, solvent assisted micro-contact molding, and micro-contact printing. For instance, the micro-contact printing process involves using a patterned

stamp made of soft material (e.g., PDMS or silicone rubber) to transfer a molecular ink onto a solid substrate. [18, 19] This method has been used to pattern monolayers of alkanethiols, proteins, chemical precursors, and other biological materials on a variety of substrates. However, it invariably requires a dedicated photolithography mask to produce inverse mask features and is limited in terms of multiple-ink and alignment registration capabilities. The generation of masks, typically by EBL, can be costly and time-consuming. Phase shift photolithography uses an elastomeric mask to modulate the phase of the ultraviolet light in a contact-mode lithography process to produce sub-100 nm features using a low-cost micrometer resolution mask. However, this method is not capable of direct patterning of chemical or biological materials.

The nanoimprinting lithography process and its variations are based on the principle of mechanically modifying a thin polymer film with a stamp containing a nanoscale pattern. A powerful NIL technique was developed earlier by Chou [20-23] that provides 25 nm or smaller structures with high aspect ratios. This method is potentially a high throughput mass production lithography method that has the ability to produce features as small as 5 nm. In the laser-assisted direct imprint technique, a single excimer laser pulse melts a thin surface layer of silicon, and a mold is embossed into the resulting liquid layer. The embossing time is less than 250 ns.

The dip pen nanolithography (DPN) technique (figure 8) utilizes a scanning probe microscope (SPM) tip (e.g., an atomic force microscope (AFM) tip) as a ‘nib’ or ‘pen’, a solid state substrate (e.g. gold) as ‘paper’, and molecules with a chemical affinity for the solid state substrate as ‘ink’. Capillary transport of molecules from the tip to the solid substrate is used in DPN to directly write patterns consisting of a relatively small

collection of molecules in submicrometer or nanometer dimensions. DPN can deliver relatively small amounts of a molecular substance to a substrate in a nanolithographic fashion that does not rely on a resist, a stamp, complicated processing methods, or sophisticated noncommercial instrumentation.[24-26] The deposition process involves a chemically engineered ink-and-substrate combination, and the ubiquitous nanoscale

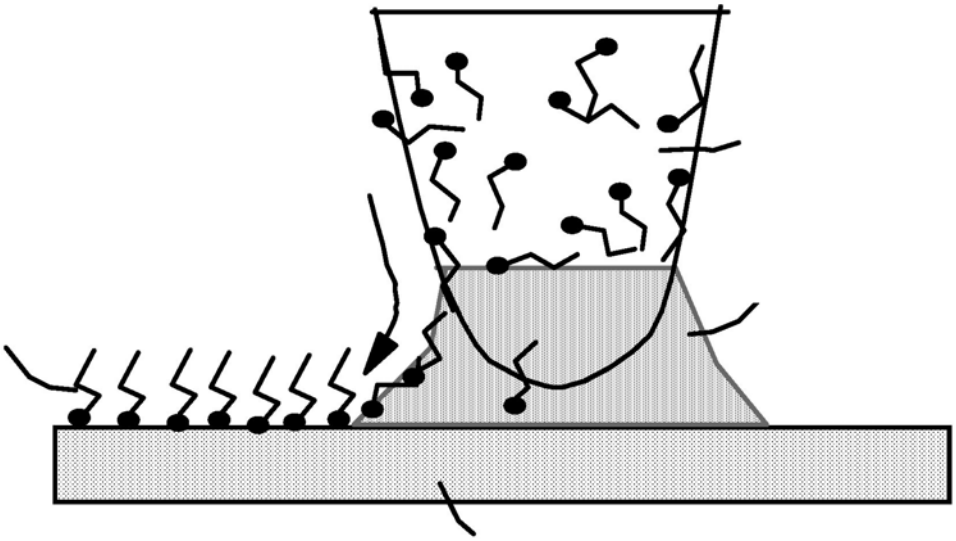

Figure 8. Schematic illustration of dip pen nanolithography technique[26]

positioning control offered by scanning probes provides the ability to produce high-quality nanolithographic patterns. DPN type techniques can be advantageous if one is trying to selectively place different types of molecules at specific sites within a particular type of nanostructure. However, this type of technology, strictly depending upon surface diffusion to deliver low-density molecules, is intrinsically a slow process. It has been difficult to deposit higher molecular weight materials (e.g., hydrocarbon polymers). It is also essentially limited to the deposition of water-compatible materials.

2.2.2 LIGA

The LIGA process is a technology developed in the Forschungszentrum Karlsruhe in Germany in 1980s. [27, 28] This is a process where three processes to fabricate a master for a metallic mold by a deep X-ray lithography, a micro metallic mold by electroforming, and replication products by injection molding and hot embossing are integrated. The LIGA technology provides unique advantages over other manufacturing methods in the fabrication of microstructures. Its schematic description and process sequence are

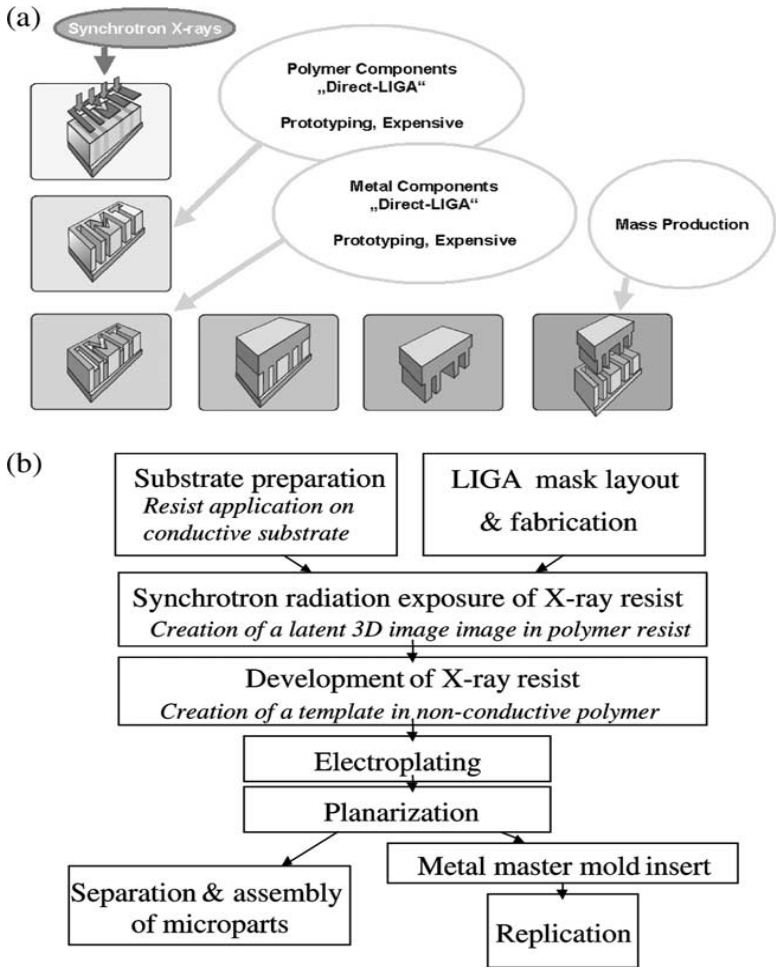

Figure 9. Illustration of LIGA a) process steps b) process sequence[29]

described in figure 9. In the first step of the LIGA process, an X-ray sensitive polymer (resist) layer up to several millimeters thick, typically polymethylmethacrylate (PMMA) is coated onto a conductive substrate. A pattern from a mask is therefore transferred into the thick resist layer via a 1:1 shadow proximity printing scheme using hard X-rays from a synchrotron radiation source. After exposure, selective dissolution of the chemically modified irradiated parts of the resist layer in a chemical developer results in a polymeric relief replica of the mask pattern. Then, depending on the material and number of parts selected for the final product, different fabrication routes can be chosen, which may include further steps of microreplication through electroforming and/or a variety of molding techniques (injection molding, embossing, casting, compression molding, etc)

2.2.3 Other techniques

Other approaches have also been proposed/employed in attempts to fabricate 3-D structures on the nanoscale level. Spherical lenses were obtained by reactive ion etching (RIE) following a photolithographic process involving localized oxidation[30], and electrodeposition was used along with a special patterning and biasing of the seed layer to achieve 3-D shapes.[31] Some direct etching techniques were proposed as well to fashion 3-D structures including laser-assisted chemical etching[32], ultrasonic machining[33], electro discharge machining[34], etc. Furthermore, a layer-by-layer laser-induced polymerization technique ("stereolithography") was also introduced.[35] However, all of the above employed methods were successful in fabricating 3-D structures where the feature size is in the order of microns and some of them require unconventional equipment or tools, which becomes the major obstacle for 3-D nanostructure fabrications.

Chapter 3 Objectives of the Research

The ultimate goal of this study is to develop a systematic method of fabricating nanoscale 3-D structures of arbitrary shape by using grayscale electron beam lithography and reactive ion etching, furthermore examine and demonstrate the feasibility of developing such a method. The ability of constructing 3-D nanoscale structures of arbitrary shape with high dimensional fidelity will not only contribute to efficient realization of the devices requiring such structures, but also trigger developing new devices with unconventional shape and structure that enable new functionality. Most important, it will ensure efficient processing by eliminating repeated fabrication and adjustment processes.

Chapter 4 Experimental Procedures and Simulation Analysis

One of the essential steps in fabricating nanoscale 3-D structures of arbitrary shape using EBL is to control the spatial distribution of exposure such that the target structure is achieved after development. In this study, the controllability of exposure distribution has been analyzed through computer simulation. While the remaining resist profile does not follow the exposure distribution exactly due to the nonlinearity of relationship between the exposure and developing rate, the ability to control the exposure distribution closely is essential in fabricating 3-D structures. Given a 3-D structure, a target exposure distribution required for obtaining the remaining resist profile matching the structure may be derived. Then, the spatial dose distribution leading to the exposure distribution needs to be computed.

4.1 PYRAMID and Its Simulation Results

4.1.1 PYRAMID

A hierarchical approach to proximity effect correction for binary lithography, named PYRAMID, was proposed in order to develop fast and accurate correction schemes that are generally applicable.[36] Since then, several versions of the PYRAMID approach have been implemented, including the versions for shape modification, dose modification, and heterogeneous substrates.[37-41]

The distinct features of the PYRAMID approach are:

• Its novel two-level hierarchy in both exposure estimation and correction steps, which provides a foundation for fast, accurate and flexible correction schemes.

• Its efficient use of look-up tables in exposure estimation and feature correction, which accelerates correction by orders of magnitude.

One of the main functionalities of the PYRAMID algorithm includes derivation of the dose distribution given an exposure distribution or vice versa. PYRAMID adopts a space-invariant linear system model of the lithographic process and estimates exposure by the convolution between a dose distribution and a point spread function (PSF). The PSF depicts the energy (exposure) distribution in the resist when a point is exposed. A distinct feature of the PYRAMID approach, compared to others, is that it distinguishes the short-range electron scattering from the long-range during convolution. This enables PYRAMID to find the exposure distribution in a pattern quickly and accurately.

4.1.2 Simulation on Staircase

The staircase structure contains discrete levels and sharp transitions between the adjacent levels while the polynomial structure, generated by the function includes smooth surfaces of rather arbitrary shape as shown in Figure 10. The substrate system consists of 500 *n*m PMMA on Si, and the beam energy is 50 keV. In the simulation, the pixel interval is assumed to be 5 *n*m. The domain of each structure is partitioned, in one dimension, into a set of thin and long rectangles where each rectangle is 5 pixels wide (or 25 *n*m). That is, dose is controlled spatially at the resolution of 25 *n*m. Two exposure distributions are considered, uncorrected and corrected. The uncorrected exposure distribution is obtained by setting the dose distribution linearly proportional to the shape

of structure. On the other hand, for the corrected exposure distribution, the dose is computed by using the PYRAMID program.

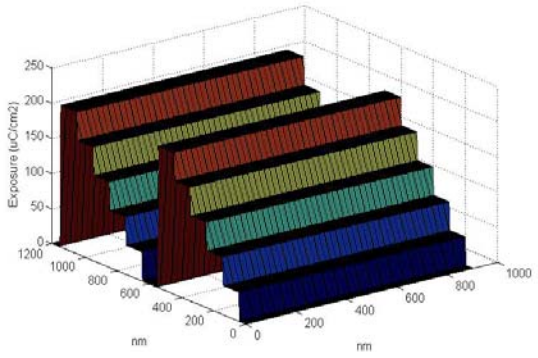

Figure 10. Target exposure distributions of Staircase structure

In Figure 11, the cross-sections of the exposure distributions are provided for more detailed comparisons. It is observed that the uncorrected exposure distribution has a larger error at the peaks and valleys than on the slopes.

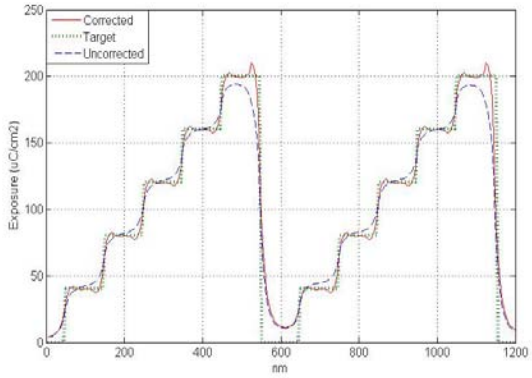

Figure 11. Cross-sections of exposure distributions of Staircase structure

In Figure 12, the 3-D plots of the uncorrected and corrected exposure distributions are provided for the two structures. It is clearly seen in Figure 12-(a) that the steps are blurred and the sharp transitions between the adjacent steps are mostly lost. However, as can be seen in Figure 12-(b), the corrected exposure distribution preserves most of the

feature shapes and is significantly closer to the target exposure distribution though the exposure error is substantial in the transition and boundary regions.

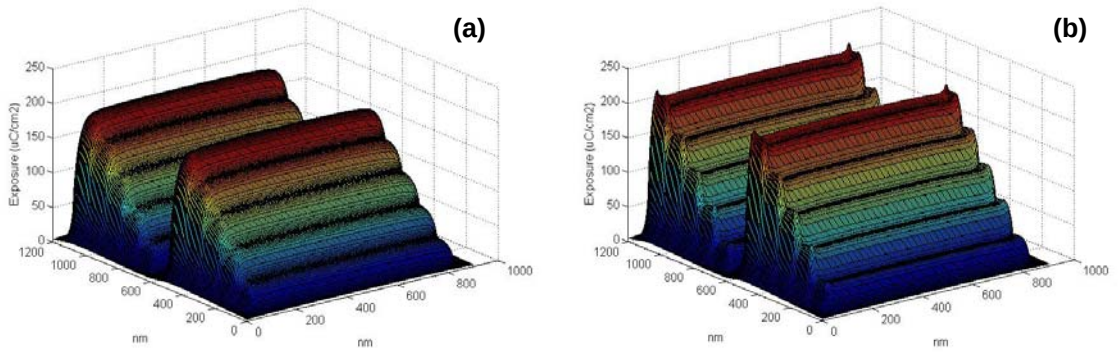

Figure 12: Uncorrected and corrected exposure distributions: (a) Staircase (uncorrected) (b) Staircase (corrected)

4.1.3 Simulation on Mirror Staircase

Since the mirror staircase structure is geometrically symmetrical to its predecessor, the simulation process then is omitted here.

4.1.4 Simulation on Polynomial structure

The target polynomial pattern is shown in Figure 13, which may be represented by $f(x, y) = p(x)$, where $p(x)$ is a 4^{th} order polynomial. It was designed to possess smooth surfaces of arbitrary shape rather than discrete levels and sharp transitions. The shape has a maximum depth of approximately 60 nm with two separate smooth, nanoscale furrow features. The pattern width was chosen to be 2.5 um to avoid any mass transfer issues in the Si etching processes. The domain (x,y) of the pattern was partitioned in the x dimension into 25 thin rectangles of 100 nm x 10 μm each where a dose is assigned to each rectangle.

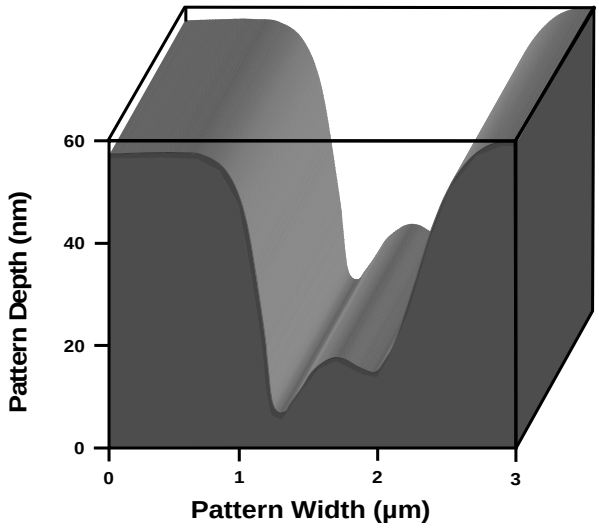

Figure 13. Schematic representation of the desired polynomial structure

The target exposure distribution was derived by sampling *p(x)* at the interval of 100 nm, i.e., it is linearly proportional to *p(x)*. Then, the PYRAMID algorithm was used to compute the dose distribution, shown in Figure. 14-(a), required to achieve the exposure distribution. The actual exposure distribution estimated by the PYRAMID algorithm is

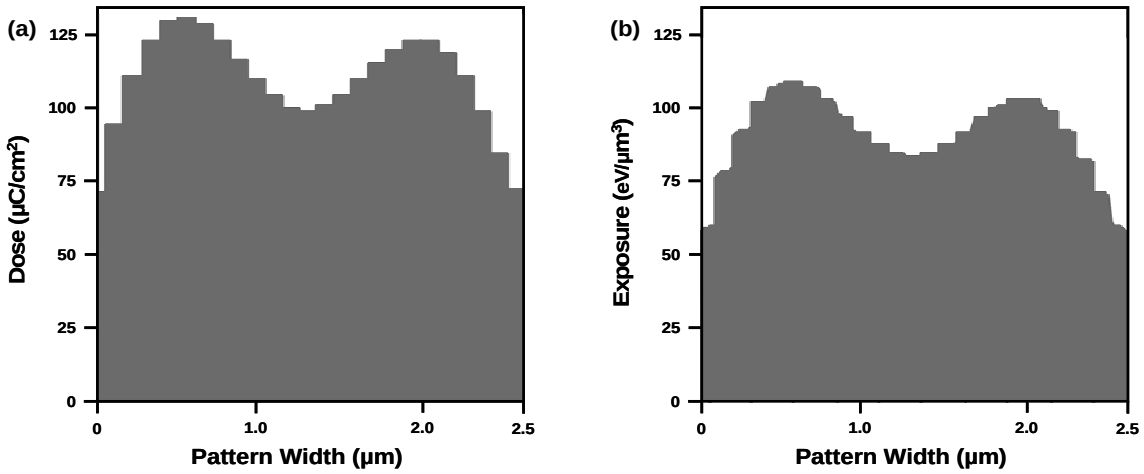

Figure 14. Pattern profiles of the target spatial dose distribution (a) and the actual exposure distribution (b) determined by PYRAMID

shown in figure. 14-(b). Though the (estimated) exposure distribution shows discrete levels, the resulting resist profile would be smooth due to the proximity effect and isotropic nature of the developing process.

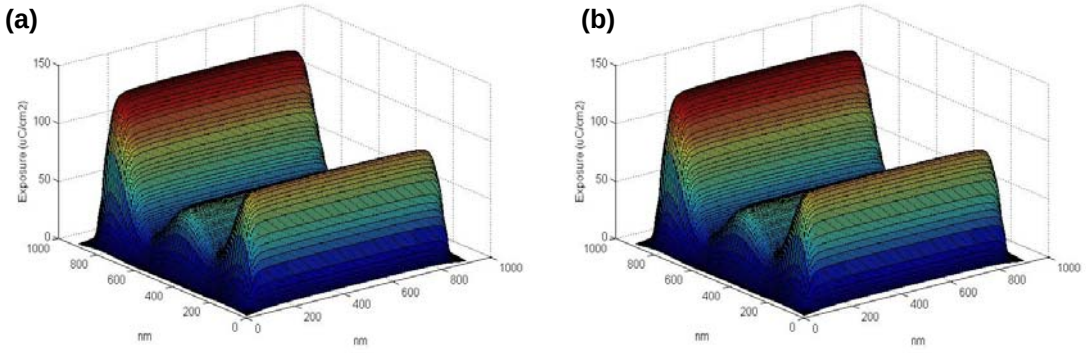

Figure 15: Uncorrected and corrected exposure distributions: (a) Polynomial (uncorrected), and (b) Polynomial (corrected)

From Figures 15-(a) and (b), it is seen that the uncorrected exposure distribution for the polynomial structure is deviated from the target one substantially more than the corrected one. That is, spatial dose control is needed even for smooth structures in order to achieve their target exposure distributions.

4.2 Design of Experiments

Design of Experiments (DOE) was used to further analyze the influence of individual parameter and their interactions involved in our study with respect to achieving and predicting optimum fabrication results. This methodology is rather useful and reliable for scientists and engineers especially when abundant amount of experimental data are to be collected. The nature of this method lies in that it applies a well-studied and commonly used conception in statistics, linear regression, to evaluate and analyze tons of data

collected and then make a reasonable prediction based upon the statistical trend of as-mentioned data. The application of this method in our study by utilizing software Design Expert 7.0 will be illustrated in chapter 5.

4.3 Fabrication and Characterization of various arbitrary 3-D structures

4.3.1 Staircase

Polymethylmethacrylate(PMMA) 950K resist was chosen to imprint the desired pattern in a (100) Si wafer. The process began first with cleaning the wafer with acetone (30 s), followed by alcohol (30 s), rinsing with DI water (1 min), and then dehydration at 120 °C for 90 min. The PMMA resist was then spun on using a speed of 6000 rpm for 45 s to achieve a thickness of approximately 100nm. The wafer was then baked at 180℃ for 5 mins to evaporate the solvent. The thickness of the PMMA resist after the spin-coating was confirmed with a calibrated ellipsometer. The e-beam lithography was performed at 30 kV on a JEOL 7000F field-emission scanning electron microscope with an integrated Nabity nanometer pattern generation system (NPGS-60). The e-beam lithography system used here mainly consists of four parts shown in Figure 16: A) Field-emission scanning electron microscope, B) high accuracy amperemeter, C) beam blanker and D) NPGS. The dose distribution in Fig. 12-(b) was imported into the NPGS and written into the PMMA resist. After exposure, the samples were developed at room temperature in an ultrasonic bath using a Methyl Isobutyl Ketone: Isopropyl Alcohol (MIBK: IPA) =1:3 developer. This was followed by rinsing with methanol and then blow drying with pure N_2 gas. The structures generated in the resist were characterized by atomic force microscopy with cantilevers possessing a vertical resolution of 10 nm. Reactive ion etching (RIE) was

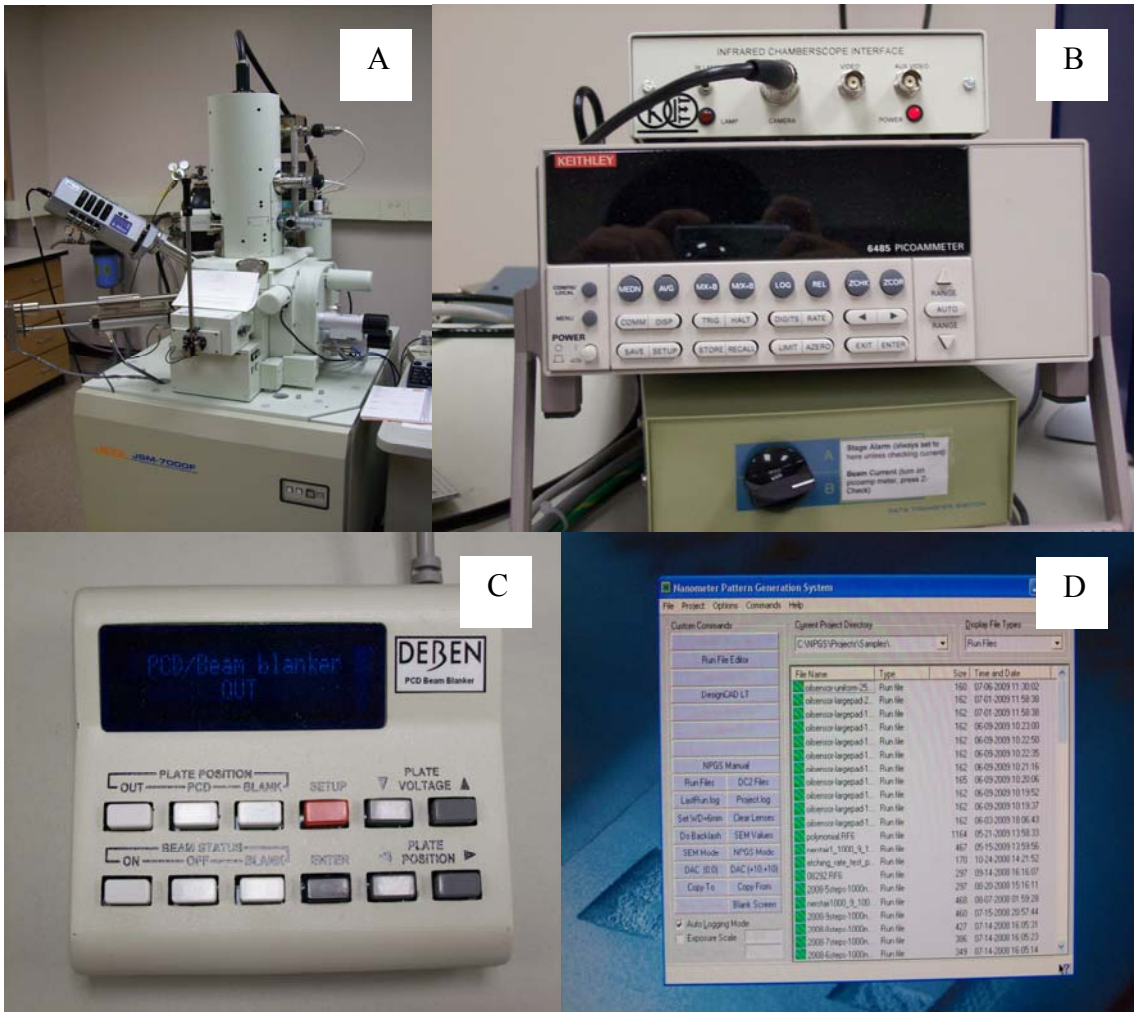

Figure 16. Four components a) Field-emission scanning electron microscope b) high accuracy amperemeter c) beam blanker d) NPGS

employed to transfer the pattern from PMMA resist to the Si wafer. The plasma etching was performed under 600W of power in an SF_6/O_2 gas mixture with their flow ratio as 10:1. Following etching, the samples were immediately cleaned with acetone and methanol to remove any residual. The staircase structures in the Si were then characterized by AFM.

4.3.2 Mirror Staircase

The fabrication process of mirror staircase was performed in a same fashion as it of staircase structure on PMMA, except some extent modification of the dose distribution according to PYRAMID simulation results.

4.3.3 Polynomial Structure

The dose distribution and pattern geometry were redesigned by PYRAMID on polynomial structures due to its unique geometry characteristic property. The fabrication process of polynomial structure was then conducted in a same fashion as it of staircase on PMMA. The patterns were transferred onto Si substrate by RIE eventually.

Chapter 5 Results and Discussion

In this chapter, we first are going to discuss the influence of different experimental factors on fabrication process. In addition, statistic analysis will be employed to indicate the significant factors and predict optimal results based upon chosen factors.

5.1 Parametric effect on fabrication process

5.1.1 Dose coefficient (DF)

Dose coefficients for each of target structure were found to play an important role in determining pattern's geometry, which is very sensitive especially when referring to

Table 1. Seven different dose coefficients used on mirror staircase structure

	1st Step	2nd Step	3rd Step	4th Step	5th Step	6th Step	7th Step	8th Step	9th Step
DF 1	0.45	0.68	0.83	0.98	1.20	0.98	0.83	0.68	0.45
DF 2	0.45	0.70	0.80	0.95	1.20	0.95	0.80	0.70	0.45
DF 3	0.50	0.71	0.84	0.97	1.20	0.97	0.84	0.71	0.50
DF 4	0.46	0.71	0.82	0.95	1.20	0.95	0.82	0.71	0.46
DF 5	0.48	0.72	0.83	0.96	1.20	0.96	0.83	0.72	0.48
DF 6	0.50	0.74	0.84	0.97	1.17	0.97	0.84	0.74	0.50
DF 7	0.54	0.77	0.87	0.99	1.17	0.99	0.87	0.77	0.54

mirror staircase structure. In table 1, seven different dose factors used on the mirror staircase structure in the experiments are listed and compared. As it is seen in the table, all other eight steps are symmetrically distributed around the fifth step in each dose factor and not a big difference among these dose coefficients can be literally revealed. These dose coefficients are also plotted as a WATERFALL shape in one graph shown in Figure 17 to demonstrate their discrepancies.

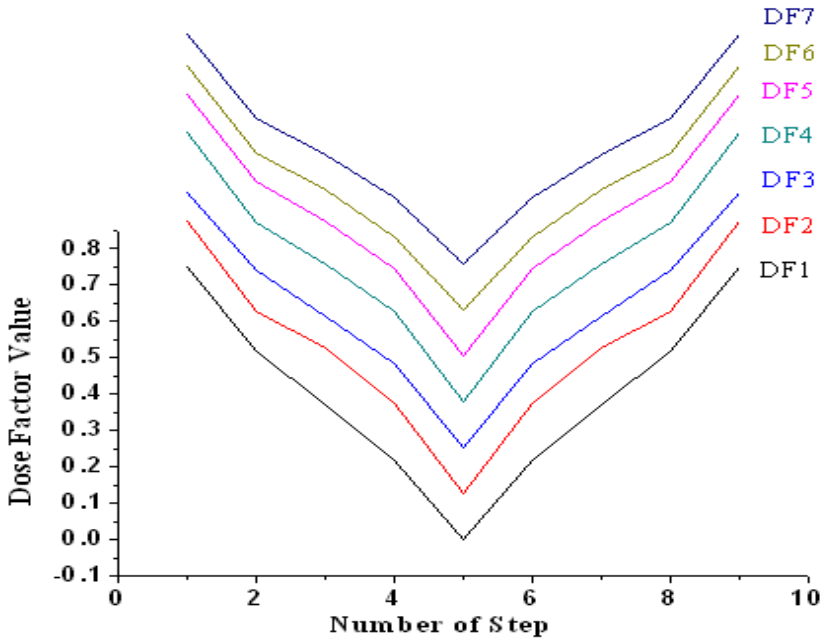

Figure 17. Schematic drawing of seven different dose coefficients on mirror staircase structure

Accordingly, the fabrication results of mirror staircase structures are given in figure 18 to verify the pattern geometry determination effect of dose coefficient. When dose factor changes from 1 to 3, the contour of the pattern experience a concave shape transition when fabrication step goes deeper. On the other hand, when does factors changes from 5

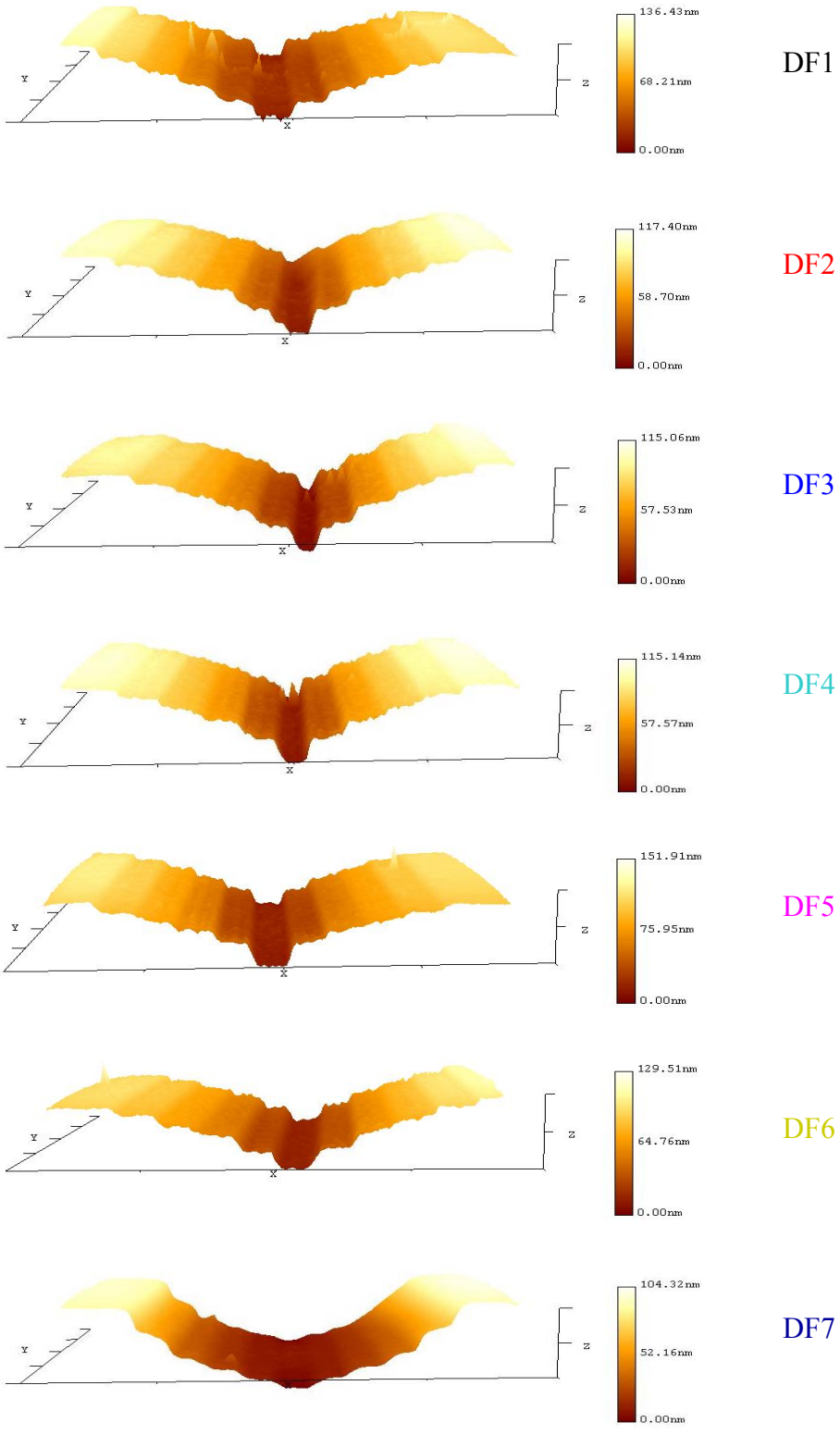

Figure 18. 3-D graphs of AFM mirror staircase structures with different dose coefficient

to 7, an obviously convex shape transition can be observed especially on the pattern with dose factor 7 when the fabrication depth goes deeper. These interesting fabrication results indicate dose factor plays an important role in determining the geometry of target structure and appear a significant controllability as well. Compare figure 17 with figure 18, it is concluded that the fabrication results are little incompatible with the dose factor change tendency, which implies there may be other factors affecting the fabrication results as well.

5.1.1 Base dose (BD)

The influence of base dose on fabrication results is obvious in terms of pattern geometry and resolution and illustrated in figure 19. The pattern geometry and resolution are well improved when the base dose used is doubled from 25 to 50 to 100. To understand this phenomenon, it needs to refer to the interaction between electron beam and photoresist, herein, PMMA and developing process. When electron beam emits on the photoresist, resist atoms will absorb energy not only from incident electrons, also called primary electrons but also from forward scattered electrons and backscattered electrons which are generated from electron-electron interaction when incident electrons penetrate the substrate and cause polymer chain in its crosslinking network break down into small molecules. These molecules then can be easily dissolved by a developer to exposure pattern. [42] When this mechanism is applied to explain the phenomenon in Figure 19, it is apparent that whether the polymer chain can be broken into small pieces and then dissolved by a developer depends significantly on the strength of incident

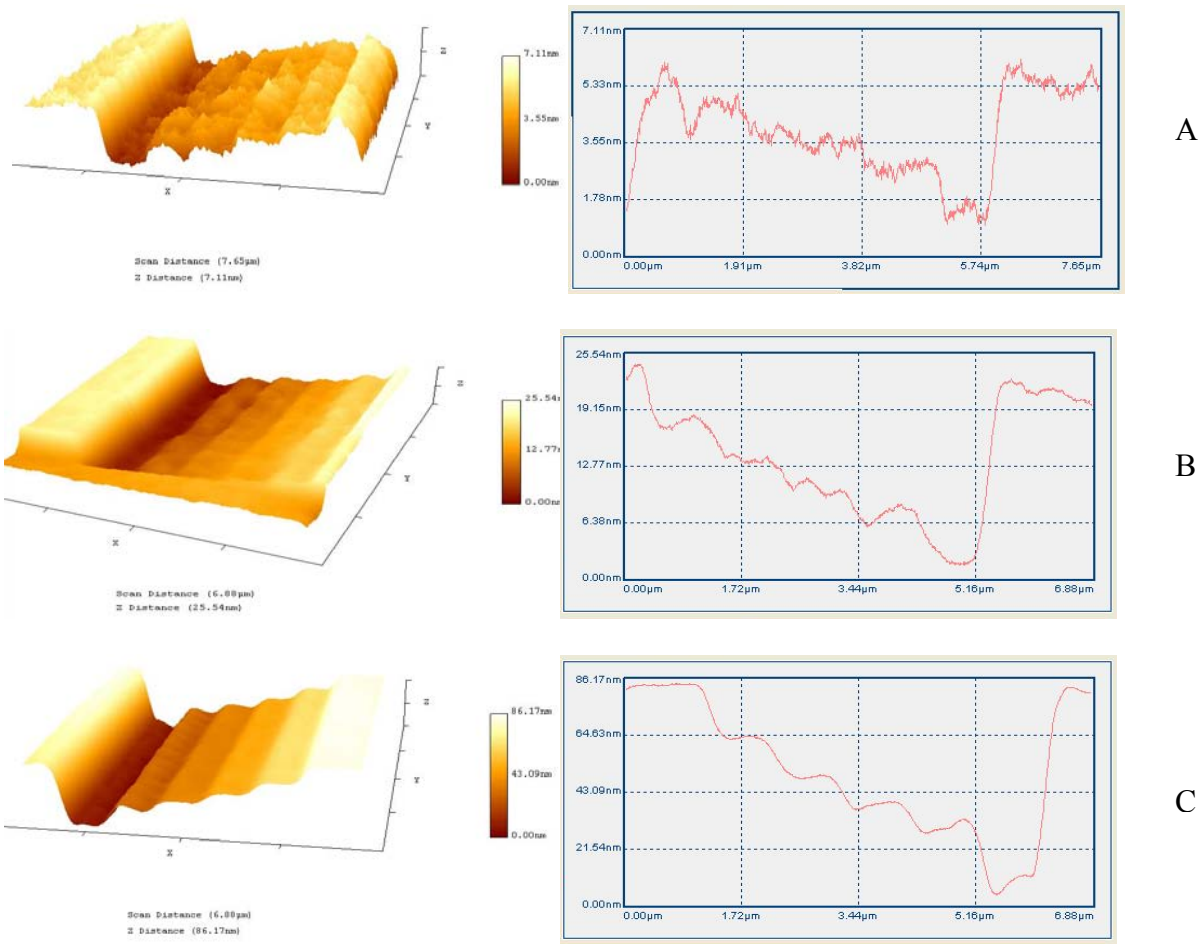

Figure 19. 3-D and profile AFM graphs of staircase pattern fabricated with various base dose

electron beam. In other words, the higher intensity of the beam, the easier to break down the polymer chain, the better geometry and resolution of the pattern.

5.1.3 Spot size (SS)

The fabrication results showed in figure 20 do not appear a big difference in terms of geometry when we only change the spot size, namely the diameter of electron beam emitted from the SEM in our experiments. The surface of all patterns look similar and

smooth, which indicates the spot size may has little influence on fabrication results in terms of pattern geometry and resolution. However, the overall height and root mean square (RMS) roughness of 5 steps in different sample varies a little from one to another

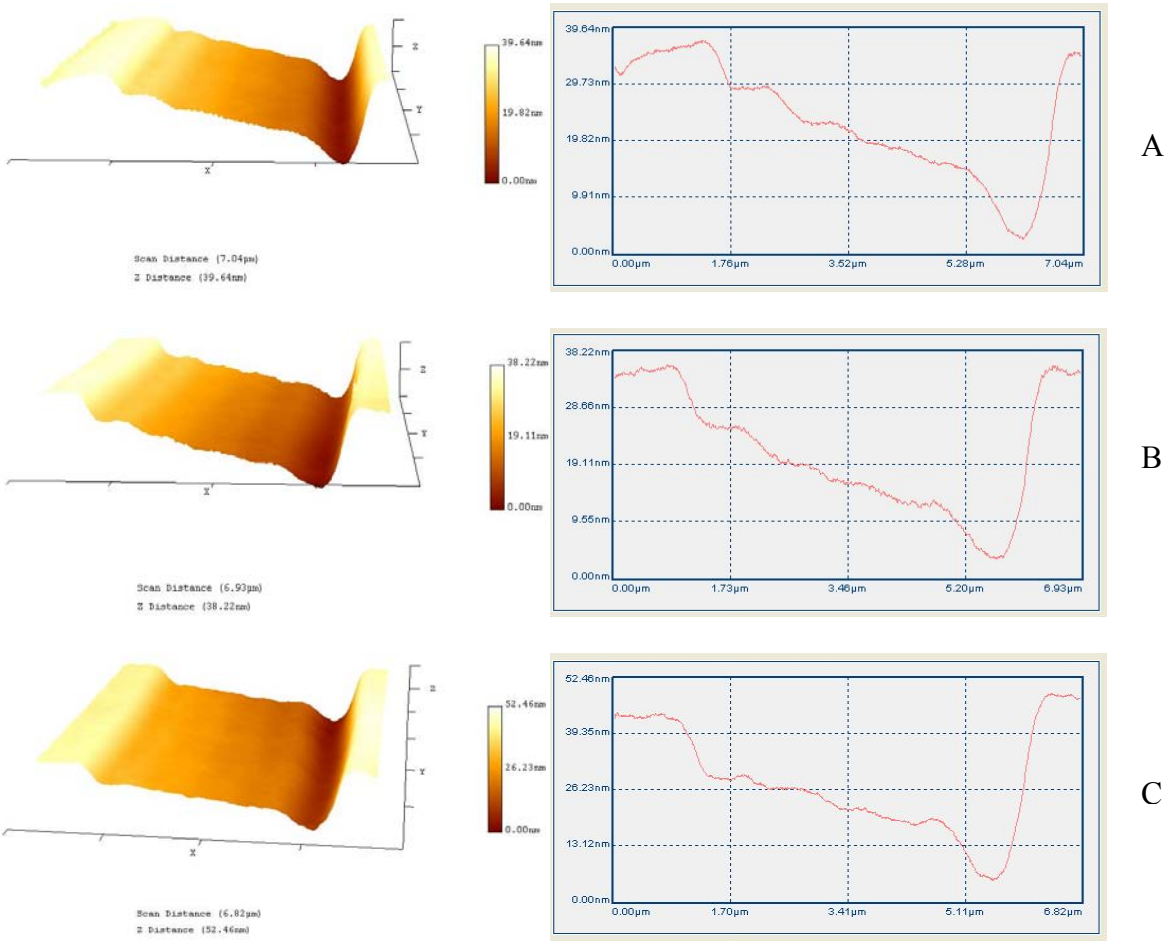

Figure 20. 3-D and profile AFM graphs of staircase pattern fabricated with various spot size

case, which are illustrated in table 2 as well as their standard deviation. As it is seen that the standard deviation for overall height and RMS roughness of three samples are 4.89%

Table 2. The overall height and RMS roughness of samples with different spot size

	Overall Height (nm)	Standard Deviation (%)	RMS Roughness (nm)	Standard Deviation (%)
Sample 1	33.28		7.49	
Sample 2	29.45	4.89	6.13	1.33
Sample 3	23.56		8.80	

and 1.33% respectively, which further confirms our previous proposition statistically since the standard deviation less than 5% is set acceptable in our experiments.

5.1.4 Line spacing (LS)

An additional aspect observed was the surface roughness of each step, which became progressively worse with depth. Furthermore, the peaks and valleys on each step appeared to exhibit some periodicity. To investigate this issue the spot size was varied systematically to determine whether the pattern is caused by the exposure line spacing. line spacing was varied from 25x25 nm to 200x200 nm and their influence is detailed in figure 21. There is a clear transition in the pattern from spacing of 100x100 nm to 50x50 nm, where the array breaks down and the surface possesses a periodic roughness. It is interesting to note that when the spacing drops to 25x25 nm the pattern of beaks and valleys becomes random. Additional spacing between the 50x50 nm and 100x100 nm were performed and a transition was seen between 80x80 nm and 90x90 nm in figure 22. It is clear here that even at 80x80 nm the exposed areas do not overlap, yet the pattern is

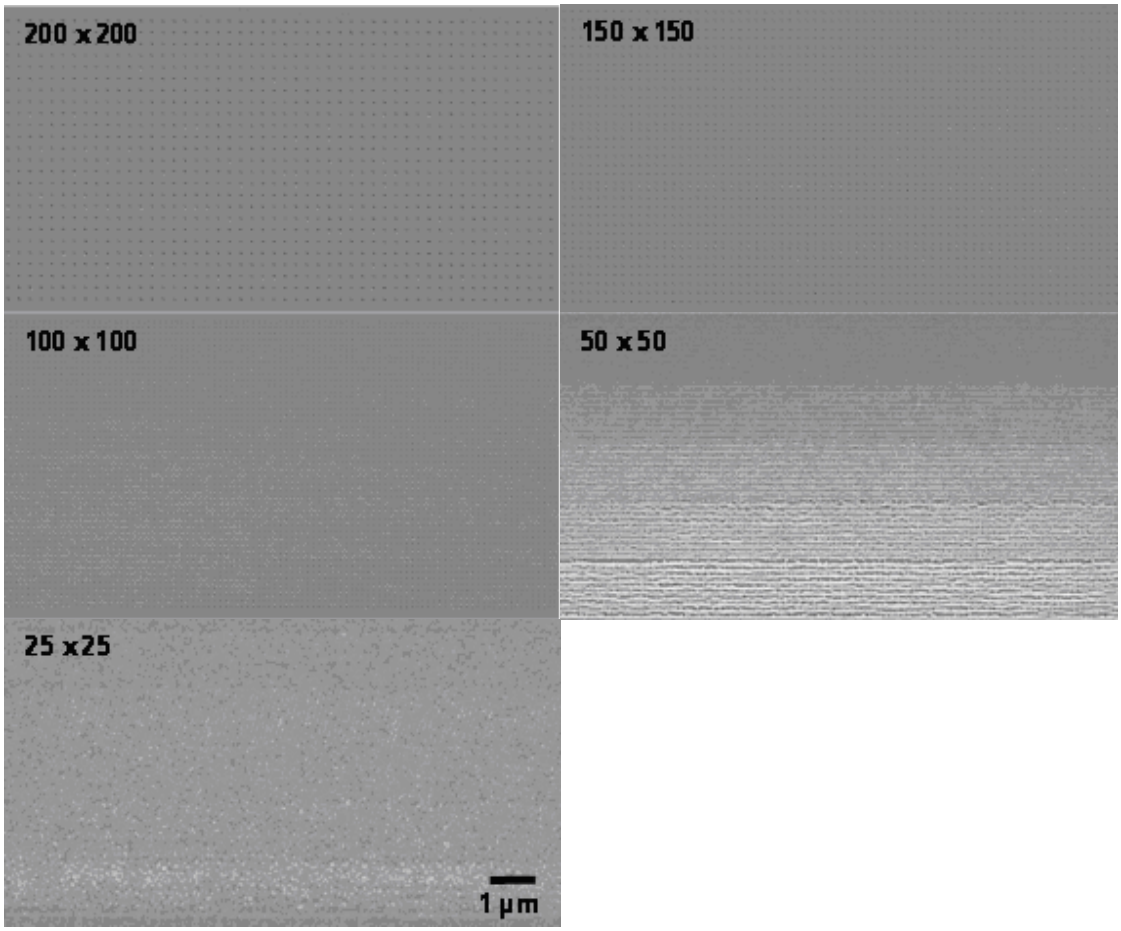

Figure. 21: Scanning electron micrographs illustrating the effect of spot spacing on the patterns

becoming distorted. This seems to be indicative of swelling of the resist during development as observed by other researchers. To mitigate this issue we plan to perform a prebake of the exposed resist and dilute the developer solution as well as perform the process in an ultrasonic bath.

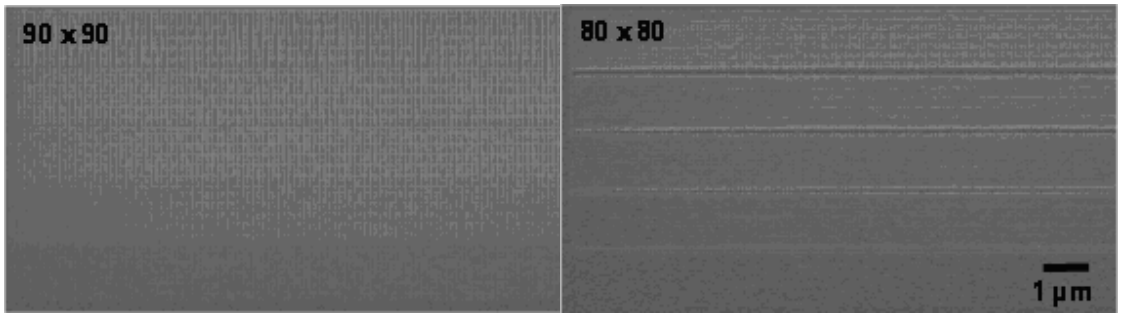

Figure. 22**:** Scanning electron micrographs illustrating the beginning transition to surface roughening

5.1.5 Developing time (DT)

As we discussed in 5.1.2, patterns need to be developed in a specific chemical, namely developer after exposure. The function of developer is to dissolve those small molecules created by polymer chain scission. Then, developing time and developer concentration should be considered as a significant factor in determining pattern geometry and resolution according to this chemical reaction. The results of staircase patterns developed at various time are demonstrated in figure 23 below. It is seen that the experimental

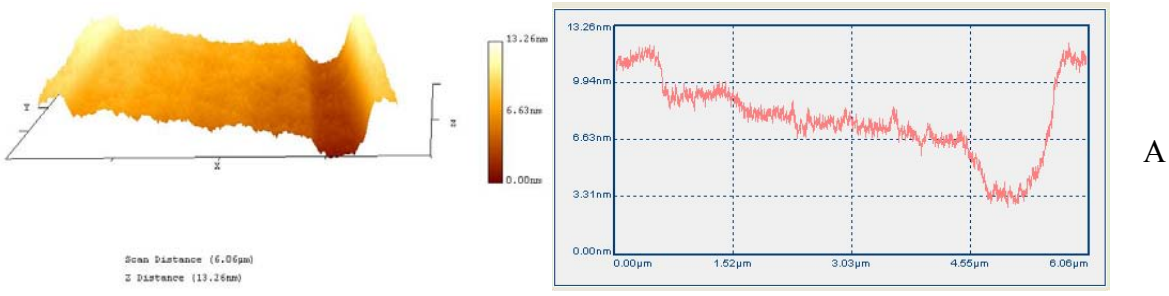

A

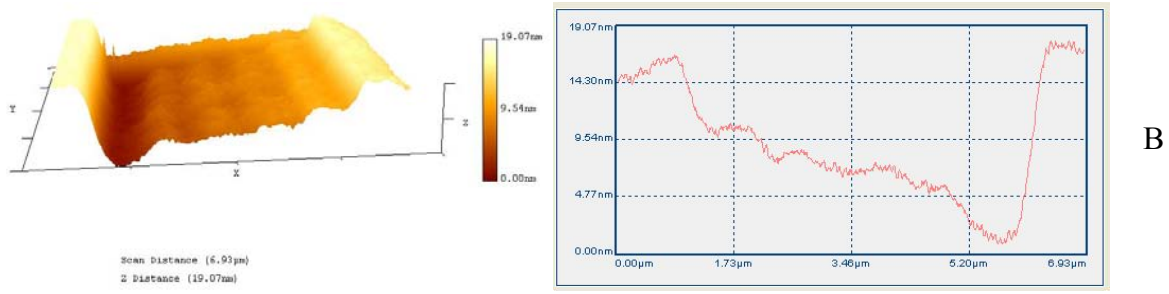

B

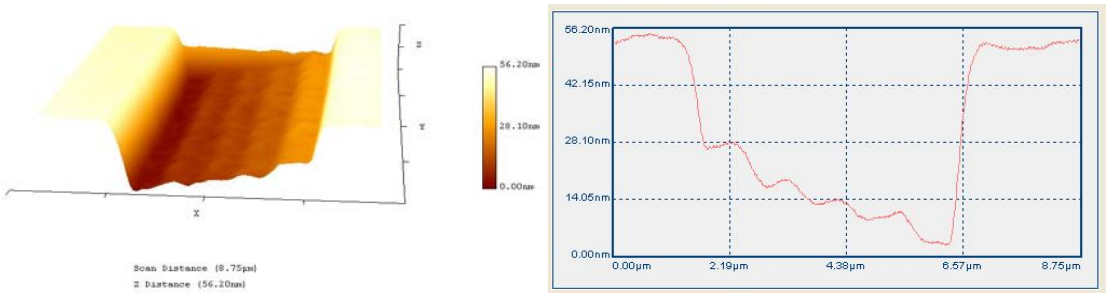

C

Figure 23. 3-D and profile AFM graphs of staircase pattern fabricated with various developing time

results are in a good agreement with theoretical analysis above. Not only the overall height of 5 steps goes deeper but also the feature and the contour of the pattern becomes clearer and smoother when increasing the developing time from 50s to 500s. What is also worth mentioning here is the overall height of 5 steps in pattern C can not reach further over 51.69 nm even though the developing time lasts 500s, which consolidates that the developing process is rather relevant to the degree of polymer chain scission. The resist without being exposed by electrons can not be developed no matter how long it is immersed in developer.

5.1.6 Developer concentration (DC)

Developer concentration turns out to be another useful factor to improve the geometry and resolution of pattern fabricated as it is evidenced in figure 24 below. Patterns developed with high developer concentration (MIKA: IPA= 1:3) and low developer

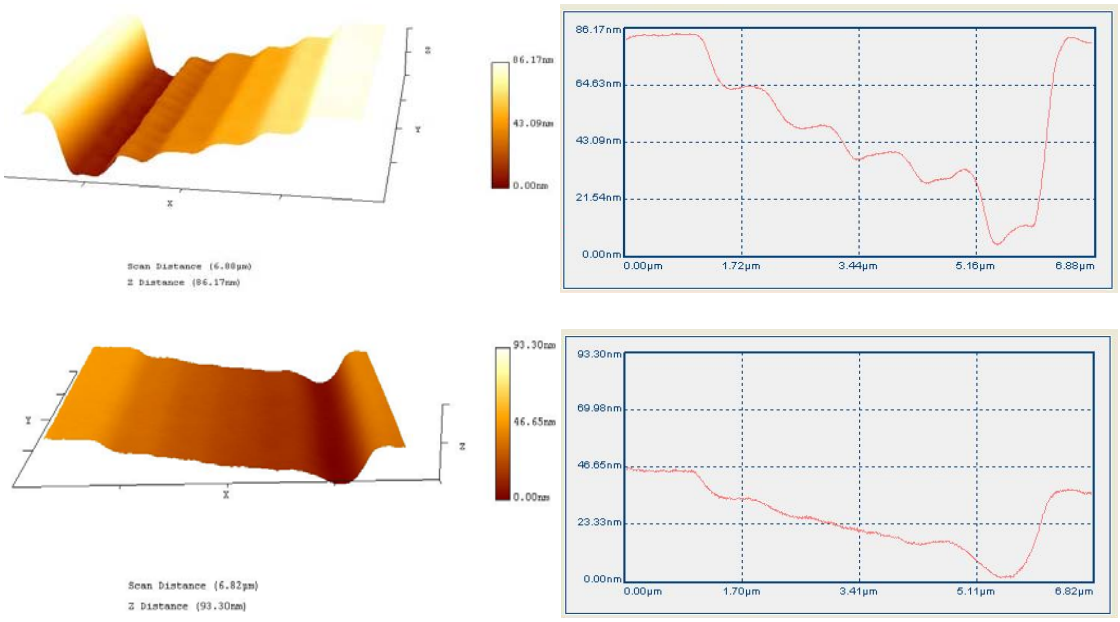

Figure 24. 3-D and profile AFM graphs of staircase pattern fabricated with various developer concentration

concentration (MIKA: IPA=1:5) are illustrated respectively and compared. All steps on pattern developed with high concentration are smooth and well recognized, which means the denser developer, the better fidelity of pattern in our experiments. However, it is not always true. Raghunath Murali et[43] investigated the performance of a series of developers in terms of contrast, sensitivity and surface roughness and they came to the conclusion that MIBK: IPA=1:1 developer is not suitable for profile depths greater than 200 nm because of its higher sensitivity to resist thickness while MIBK: IPA=1:3 developer is very sensitive to developing time. In our study, none of pattern profile depth exceeds 100nm and then the choice of our developer concentration is unrestrained by their criteria.

5.1.7 Ultrasonic agitation (UA)

It was found that ultrasonic agitation can be utilized to improve feature resolution of

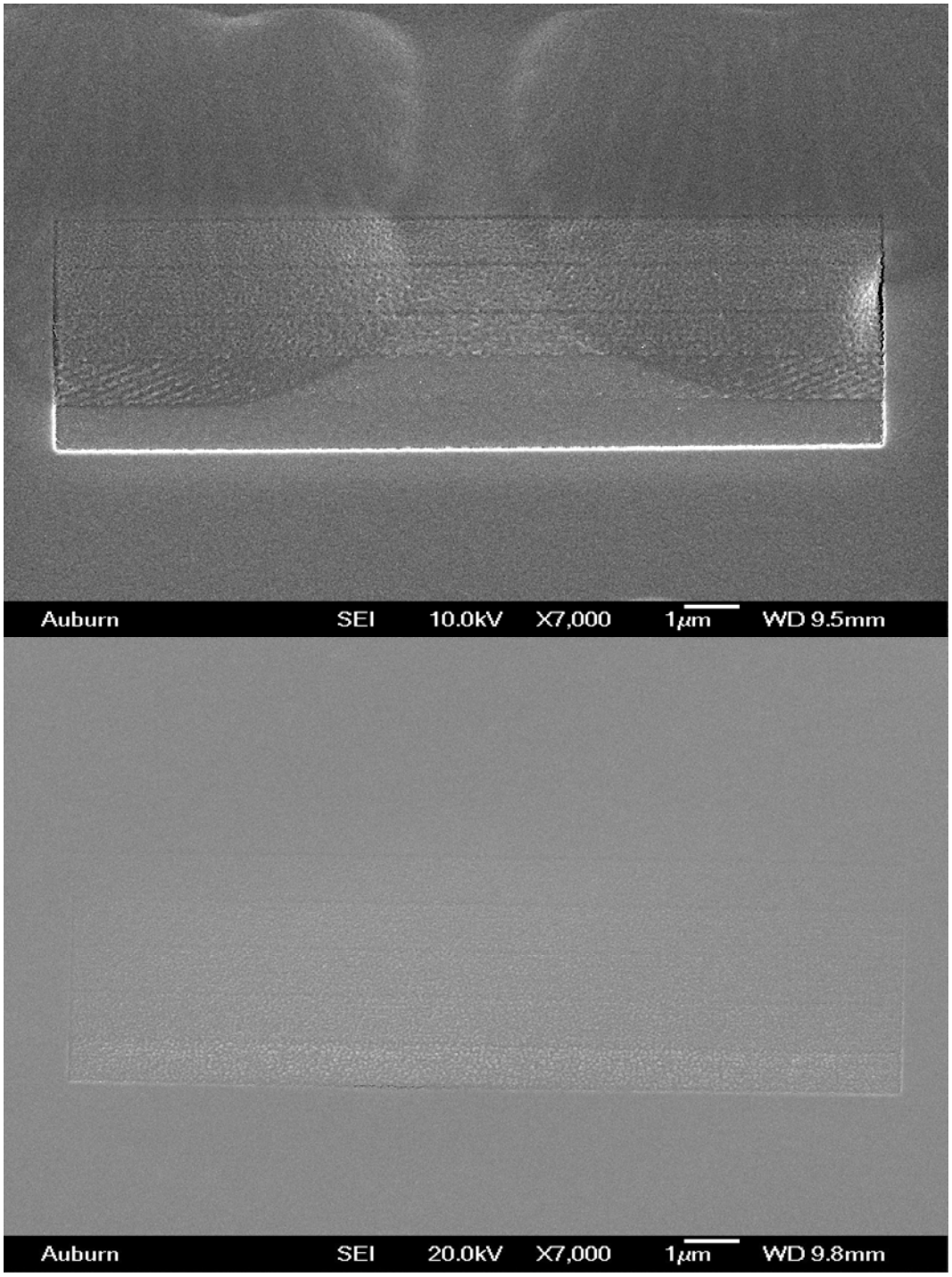

Figure 25. SEM graphs of staircase pattern fabricated without (upper) and with (lower) ultrasonic agitation

pattern fabricated when developing. The influence of ultrasonic agitation on fabrication results of staircase structure are elucidated in figure 25. It is obviously that photoresist without being processed by ultrasonic agitation appears some degree of swelling while it does not with ultrasonic agitation. According to our experiments, it turns out that the ultrasonic agitation not only plays an important role in improving resolution but also is able to shorten developing time. It is speculated that on one hand, ultrasonic agitation provides the energy compensation through the reduction of dose level of electron energy, on the other hand promotes the mixing of polymer/solvent through microstreaming effect to inhibit phase separation of two that leads to line edge roughness.

5.2 Fabrication results

In our study, three various shape 3-D nanostructures were fabricated by grayscale electron beam lithography and reactive ion etching according to their prototypes shown in figure 26 respectively. A and B represent two different staircase structures while C represents a unique polynomial structure. Herein, staircase structure is composed of 5 sets

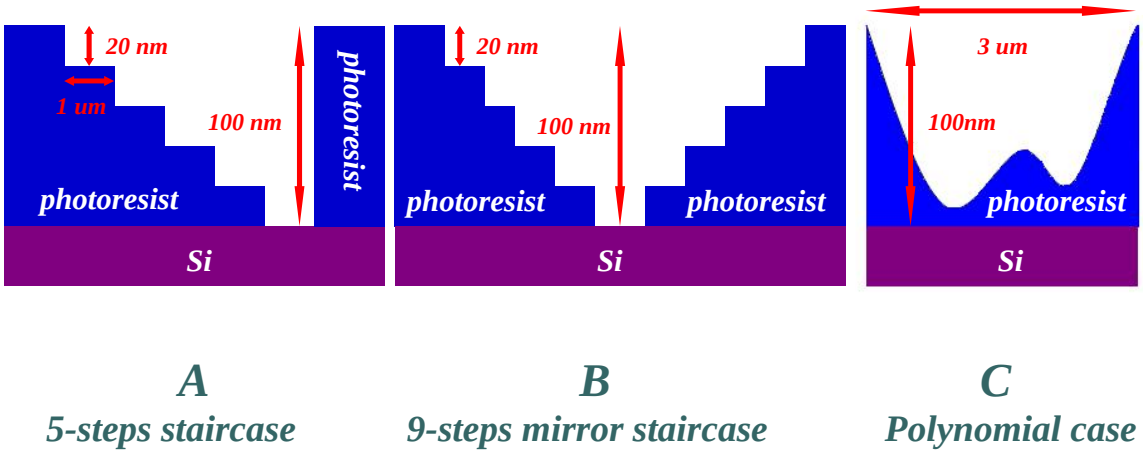

Figure 26. Prototypes for three various shape 3-D nanostructures

of same rectangles with fixed length and width while polynomial structure only has width fixed. Their optimum fabrication results are shown in figure 27 respectively.

As it is seen in figure 27, all patterns fabricated appear good feature and resolution compatible with their respective prototypes, especially on staircase and polynomial structure. However, it is obvious that the individual height of each step and overall height of all steps in staircase and mirror staircase do not match up with their original design. Instead, they are shorter than their designs in either case, which indicates the dose

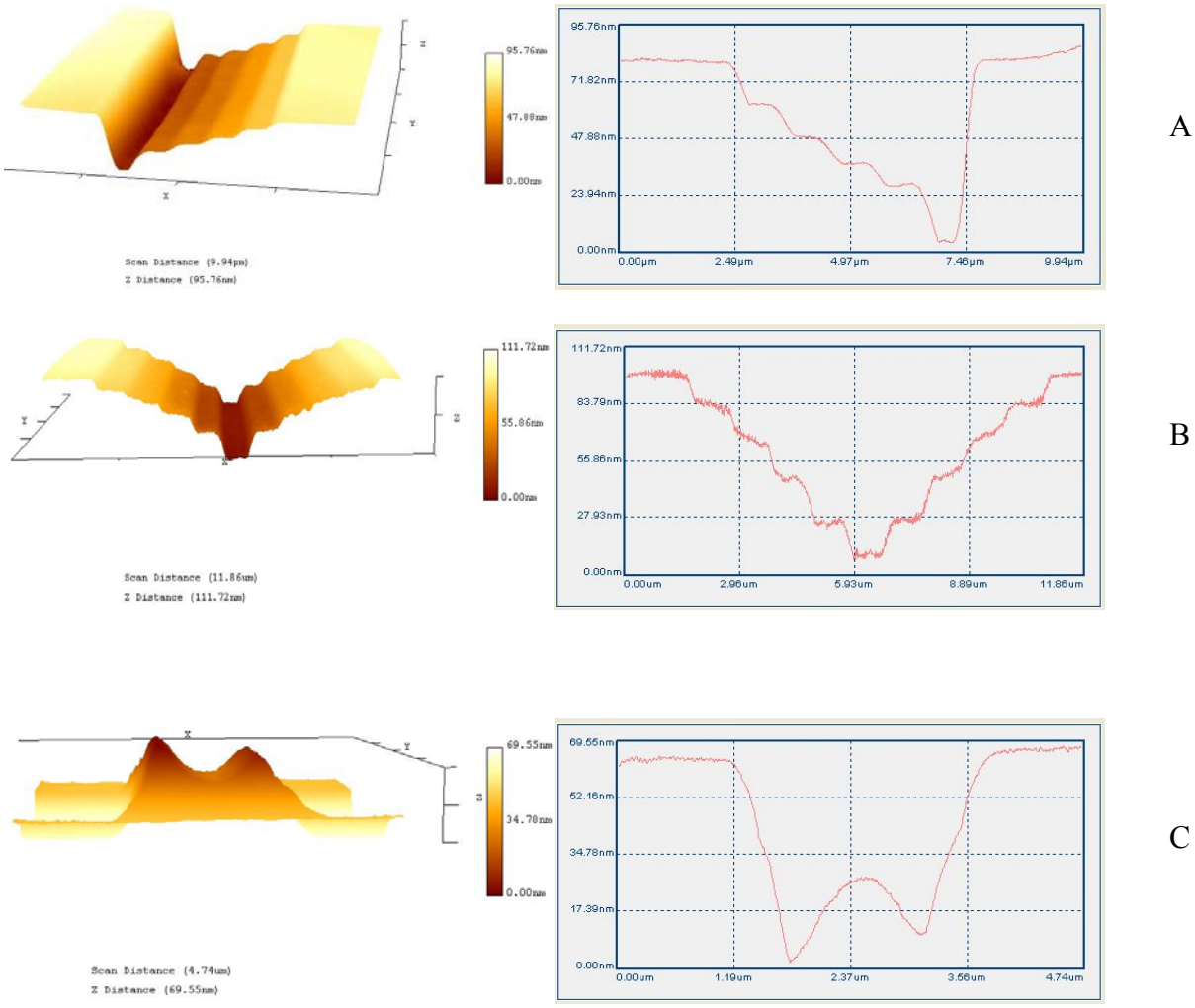

Figure 27. 3-D and profile AFM graphs of three various pattern fabricated A) Staircase B) Mirror staircase C) Polynomial structure on PMMA

exposured of each feature on photoresist is a little less than it irradiated. The plausible reason for this is either that insufficient electron beam energy is used in our lithography system due to low accelerating voltage (30 keV) as other researchers normally uses high energy electron beam to avoid forward-scattering and backscattering electrons, [42, 43] or the dose factor is not appropriately designed judging by the uneven height of individual step in either case. What also needs to be explained is that the slope between steps is not the way it looks like but the measurement error due to inaccuracy of AFM probe. It will be significantly improved only if the resolution of 1 nm AFM probe is to be used according to the manufacturer.

In addition, the fabrication result of polynomial structure on Si substrate is shown in figure 28 to make a comparison with it on PMMA. In figure 27 C, the height and width of the entire polynomial structure pattern were 63.2 nm and 2.56 μm respectively. The surface of the polynomial structure and surrounding PMMA were not ideally smooth, possessing a degree of surface roughness, root mean square (RMS) of 2.52 nm. This roughness is likely a result of non-ideal nano-transport of solvent and solute into the polymer, which can result in less defined and swollen features. Other researchers have

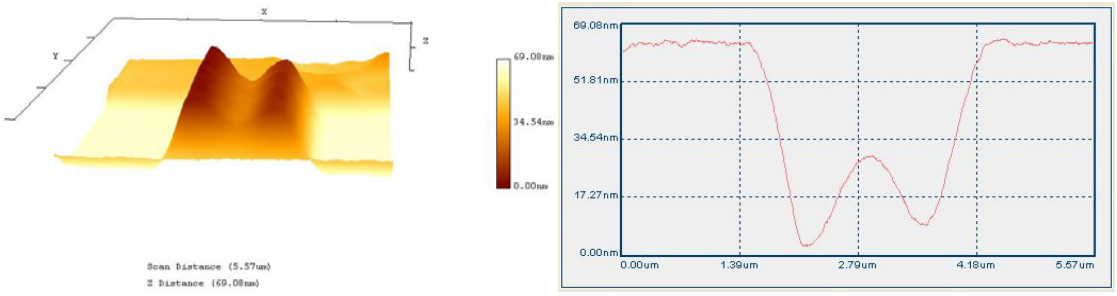

Figure 28. 3-D and profile AFM graphs of polynomial structure on Si substrate

characterized this phenomenon and demonstrated that it can be minimized by employing a higher molecular weight PMMA and ultrasonic-aided development of PMMA. [44-46] this study leveraged these techniques and obtained a rather low surface roughness, which was approximately 20 to 30 times less than the desired pattern features. As will be shown in the following results, this roughness appears to have only negligible influence on transferring the pattern into Si in figure 28. The cross sectional slice of the pattern indicates that the shape was successfully transferred into the Si substrate. The pattern depth and width of the polynomial structure were 58.2 nm and 2.71 μm respectively and matches the dimensions of the desired pattern well. The pattern profile is smoother and more uniform than that of the resist, likely due to the isotropic characteristics of fluorine-based Si etching.[47] Thus, the roughness resulting from the developing process had little to no effect on the etched pattern. Finally, the chosen etching parameters resulted in approximately a 1:1 etching rate between the PMMA resist and Si substrate. This is highly desired as maintaining the resist profile as close to the desired 3-D structure as possible and enables simplification of the pattern generation and transfer by RIE etching.

5.3 DOE analysis

5.3.1 The determination of response

In our study, five major variables, developer concentration(A), developing time(B), line spacing(C), spot size(D), base dose(E) in the lithography and develop process were chosen to perform design of experiment. Each one of the variable has at least two or three levels, which is demonstrated in table 3. As it is seen in table 3, five variables with up to

3 levels are able to generate 3*3*3*3*3*2=162 experimental runs. The number of runs continues to grow if we keep adding either variables or levels.

The response used in DOE analysis to define our experimental results is a little complicated to determine due to the goal of this study which not only needs the structure

Table 3. Five major variables and their respective levels used for DOE analysis

	Base dose(uC/cm^2)	Line spacing	Spot size (nm)	Developing time (s)	Developer concentration (MIBK:IPA)
Level 1	25	5	6	50	1:3
Level 2	50	10	8	100	1:5
Level 3	100	25	10	500	

to match with target structure as much as possible, but also to minimize the RMS roughness of it. In other words, the geometry and RMS roughness have to be satisfied simultaneously. Therefore, we designed a reasonable response, multiply factor (MF), shown in equation 1 below.

$$MF = \frac{1}{TR} X \frac{Ns}{5} X \left(\frac{1}{\sum_{i=1}^{5} (20 - SHi)^2}\right) \quad (1)$$

Herein,

MF---Multiply factor

TR---The RMS roughness of the whole pattern

Ns---Number of steps counted in the pattern

SHi---The height of the i^{th} step, namely SH1 represent the height of step1, SH2 the height of step 2, SH3 the height of step 3 etc

$\sum_{i=1}^{5}(20-SHi)^2$ ---Sum, represents the accumulation of individual step height after normalization by 20.

In this equation, the response, MF is determined by its three components, $\frac{1}{TR}$, $\frac{Ns}{5}$, and $\frac{1}{\sum_{i=1}^{5}(20-SHi)^2}$ and each components is a mathematical description and normalization of existing experiment data, such as $\frac{1}{TR}$ represents the degree of the RMS roughness of each pattern while $\frac{Ns}{5}$ represents the completeness of steps in a pattern and Sum represents the degree of individual step height close to the target structure. The response can be determined only by multiplying all of them upon geometry and RMS roughness satisfaction.

5.3.2 Software operation

Eventually, the DOE spreadsheet shown in Appendix is able to be established based upon the response we proposed above.

What is worth mentioning in this spreadsheet is that the response data are sorted in a descending order for better visualization upon MF. Meanwhile, the absence of data is due to inadequacy of measurement instrumentations. They can be ignored while the software processes the data.

5.3.3 Statistical evaluation

The analysis of variance (ANOVA) for the response MF is given in table 4 below in details. ANOVA is a statistical method used to partition the total variation into its components, one of which is the statistical difference among means. [48] The F-ratio shown in table 4 is the ratio of the component of variation attributable to a process factor divided by the component of the variation attributable to experimental error. P-value quantifies the probability of making an error by associating an effect with a given factor. DF represents the degree of freedom. The statistical significance of the process factor effects are determined by the combination of F-ratio and P-value.

Table 4. ANOVA results for MF

Source	Sum of Squares	DF	Mean Square	F Value	P value Prob > F	Significance
Model	156.81	15	10.45	24.41	< 0.0001	Yes
A	17.2	1	17.2	40.16	< 0.0001	Yes
B	13.2	1	13.2	30.82	< 0.0001	Yes
C	0.022	1	0.022	0.051	0.8226	No
D	0.28	1	0.28	0.66	0.4215	No
E	10.27	1	10.27	23.97	< 0.0001	Yes
AB	9.94	1	9.94	23.2	< 0.0001	Yes
AC	0.098	1	0.098	0.23	0.635	No
AD	0.042	1	0.042	0.098	0.7558	No
AE	0.088	1	0.088	0.21	0.6527	No
BC	2.21E-04	1	2.21E-04	5.15E-04	0.982	No
BD	5.69E-03	1	5.69E-03	0.013	0.9088	No
BE	37.1	1	37.1	86.61	< 0.0001	Yes
CD	1.28E-03	1	1.28E-03	2.98E-03	0.9567	No
CE	0.72	1	0.72	1.68	0.2014	No
DE	0.038	1	0.038	0.089	0.7665	No
R-squared=0.8971				Adj R-squared=0.8603		

As is indicated in table 4 that the model is significant and there is only a 0.01% chance that this large could occur due to noise by F-value 24.41. In this study, A, B, E, AB, BE

turn out to be significant factors as their p-values are no larger than 0.0500. C, D, AC, AD, AE, BC, BD, CD, CE, DE turn out to be insignificant factors as their p-values are larger than 0.0001.

The R-Squared term represents the percentage of the variation in the response that is explained by the deliberate variation of the factors in the course of experiments. Its value of 0.8971 is in reasonable agreement with the Adj R-Squared term value of 0.8603, which implies the as-established model and the experimental data have a very high degree of "fit".

This good fit to the observed value can be revealed graphically in figure 29 and figure 30. Figure 29 represents the plot of normality vs internally studentized residuals. As it is seen in this figure, all data points are almost located on 45° line and form a linear relation fashion even though some scatters are expected, which indicates a good fit between the model and the experimental data and thereby our design is statistically valid and viable.

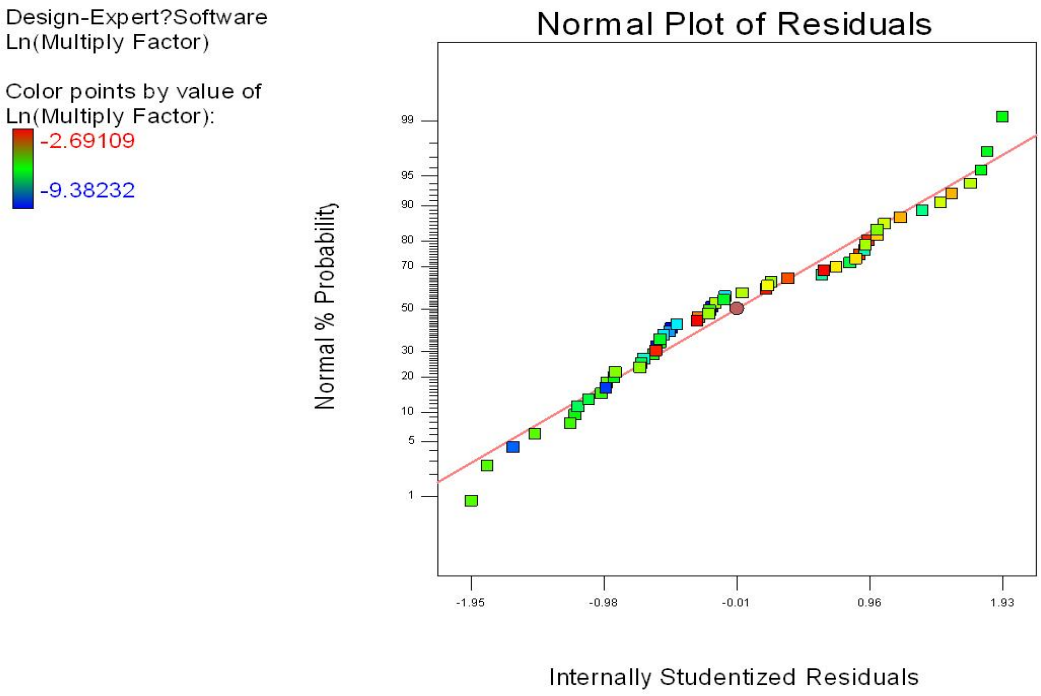

Figure 29. The Normal plot of residuals

The graph of predicted response against actual response is plotted in figure 30. Points are evenly distributed across 45° line and no outliers are found, which means there is no point which does not agree well with the rest of data when compared using the current model. In addition, by adding the insignificant factors and significant ones together, the response MF can also be modeled using equation 2 below:

MF=-12.52284+3.51857*A-0.046098*B-0.060844*C+0.24447*D+0.070058*E +0.29376*AB+0.10320*AC-0.42571*AD-0.026874*AE+1.61783E-006*BC+4.11203E -005*BD-1.58788E-004*BE-4.98145E-004*CD+5.26438E-004 (2)

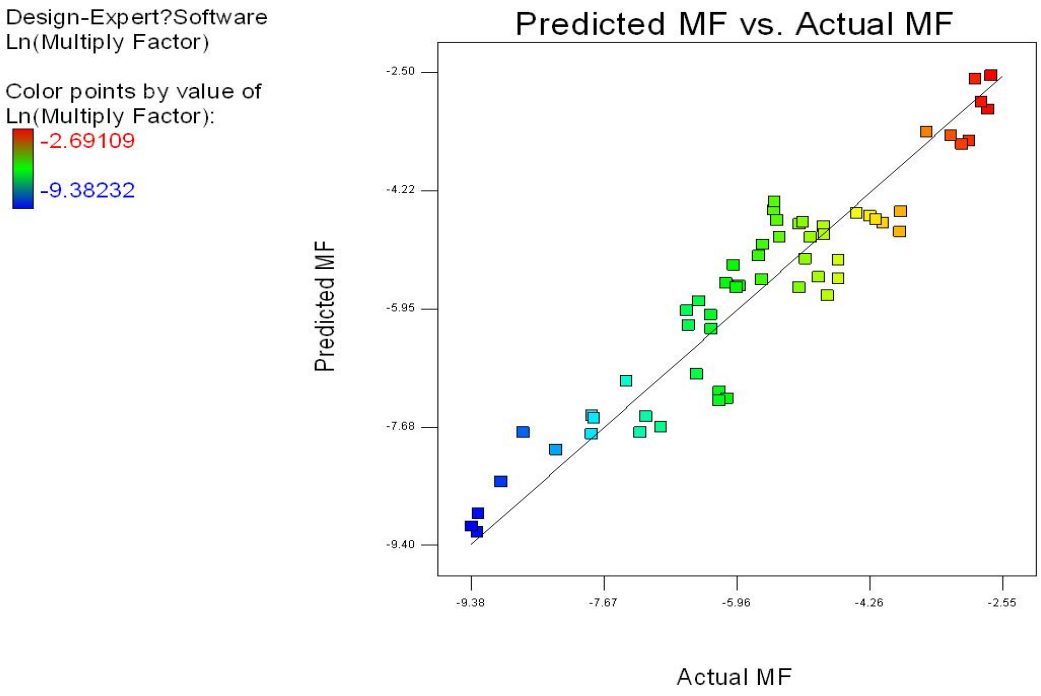

Figure 30. The plot of predicted response vs actual response

The factorial interaction of A, B and B, E under other factor values constant have been graphically demonstrated in figure 31 and figure 32 respectively. Each figure is composed of phase-like areas represented by different colors and separated by paraboloidal curves. The number on each curve represents a MF value which one can statistically obtain through a combination of A and B or B and E. As it is seen in figure 31, most of the diagram consists of red color which implies there is a high possibility that a big response, MF value can be achieved and MF increases with the increase of developer ratio and developing time. This conclusion matches well with our experimental results.

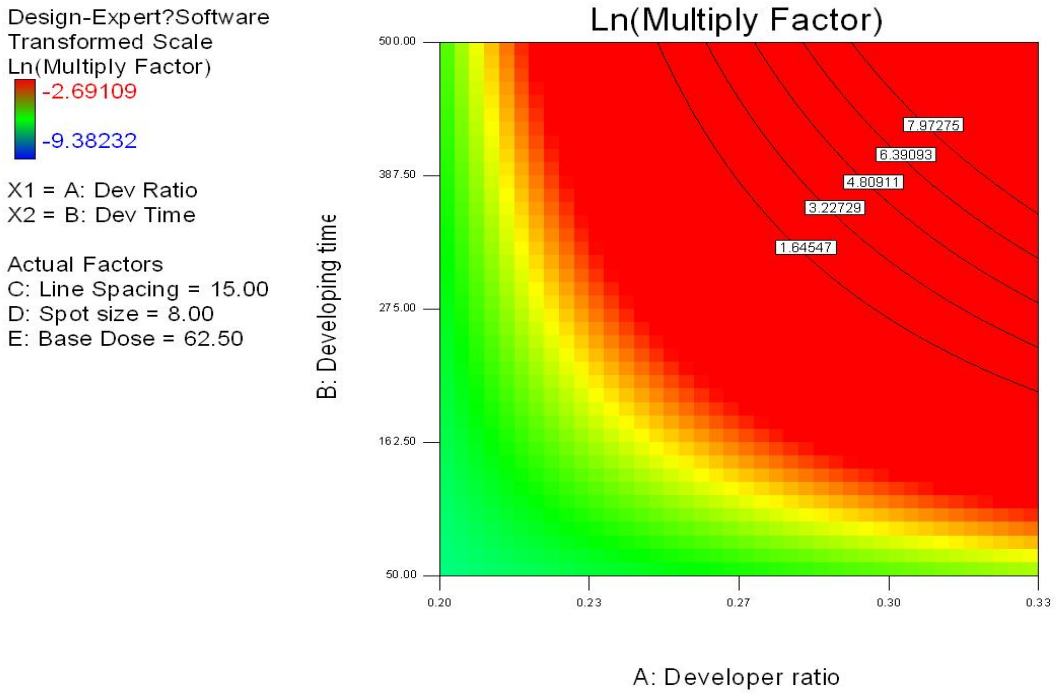

Figure 31. The factorial interaction between A and B

On the other hand, the response MF also increases while the developing time and base dose increase, as is seen in figure 32. Likewise, a high probability with which a big MF value can be achieved is indicated by the majority of red color in this graph. When figure 31 and figure 32 are compared, the difference between them lies in that DOE indicates the maximum MF that can be obtained through the interaction of B and E is 3.22729 while the maximum MF through A and B is 7.97275 as other factors are specific.

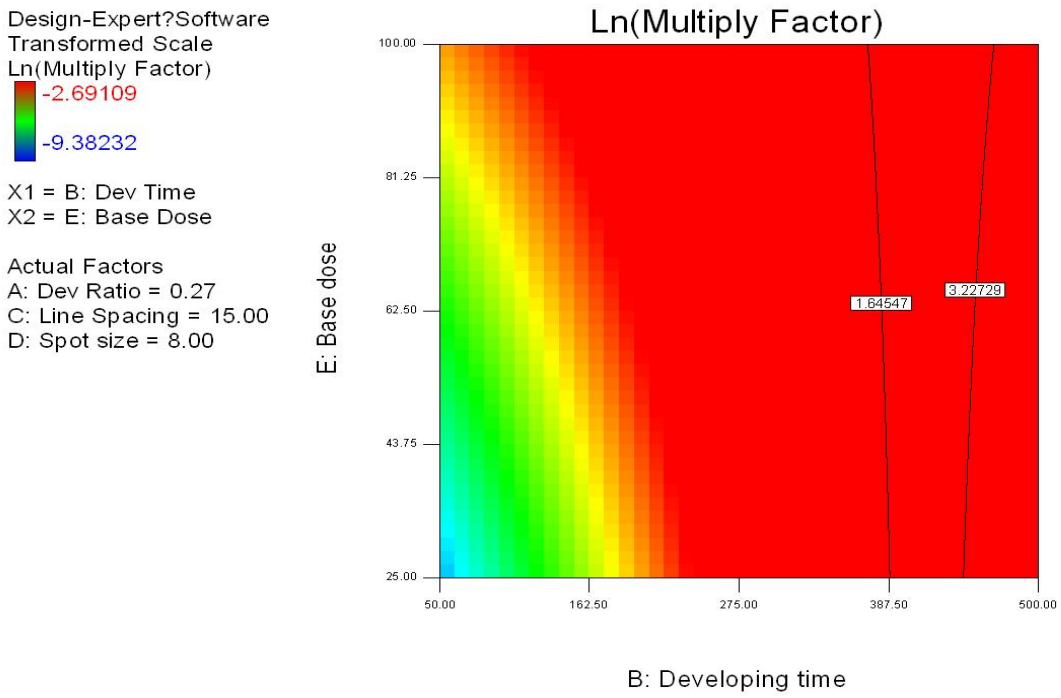

Figure 32. The factorial interaction between B and E

5.3.4 Optimization and prediction

Design of experiment is also capable of performing statistical optimization of chosen response based upon existed experimental data. The optimization solutions on our case are shown in table 5 below and they were obtained by setting all five factors values within experimental range and response maximized. Each solution represents an experimental condition to achieve optimized MF statistically. As is seen in this table, the various optimums MF can be achieved by 20 different experimental conditions by giving five factors a specific value. The desirability of them indicates a very high possibility to achieve such an optimum MF value.

Table 5. Optimization of response with respect to all factors

Number	Developing ratio	Developing time	Line spacing	Spot size	Base dose	Ln(Multiply Factor)	Desirability
1	0.33	205.5	24.28	9.97	35.91	0.603	1
2	0.33	150.36	9.68	8.89	78.62	-0.475	1
3	0.33	160.98	8.87	9.73	60.16	-0.58	1
4	0.33	180.49	5.17	7.23	28.68	-0.766	1
5	0.28	224.94	7.74	7.64	61.9	-0.785	1
6	0.33	100	25	6	100	-0.832	1
7	0.26	239.8	13.52	7.29	92.9	-1.082	1
8	0.33	147.92	6.17	9.79	57.99	-1.103	1
9	0.27	241.73	16.49	6.1	63.52	-1.235	1
10	0.33	143.56	23.06	9.8	57.26	-1.308	1
11	0.23	491.11	5.27	6	99.59	-1.369	1
12	0.33	95.76	7.03	8.41	98.17	-1.572	1
13	0.33	139.6	23.24	6.35	56.6	-1.689	1
14	0.33	162.03	23.84	6.21	30.03	-1.859	1
15	0.33	84.25	5.73	6.25	98.94	-1.914	1
16	0.33	160.1	24.95	6.03	26.9	-1.93	1
17	0.3	173.68	12.47	8.91	41.34	-2.001	1
18	0.31	76.49	24.6	9.87	98.43	-2.194	1
19	0.26	178.12	7.71	6.56	98.43	-2.393	1
20	0.33	50	25	10	100	-2.547	1

As is seen in this table, higher developer concentration is recommended in almost all solutions, except solution 11. Compared solution 11 with accordingly existing experimental condition which is listed in Appendix, the response value are -1.369 and -6.295 in each case respectively. It is confirmed that the response increases while developer concentration increases according to figure 31. Longer developing time is also suggested but limited within 250s except solution 11. Line spacing and spot size appear random change tendency whereas base dose is indicated by all solutions to be larger than 25. Compare the optimum response in the table with accordingly existing experimental condition in Appendix, it is suggested that developing time should increase significantly

while base dose has to be lowered. Developer ratio can be elevated a bit higher than it used in experiment and a little change on line spacing and spot size can be accepted.

Chapter 6 Conclusion

In this study, three various novel 3-D nanostructures, staircase, mirror staircase and polynomial case were fabricated on photoresist/Si substrate by using grayscale electron beam lithography and reactive ion etching. The proximity effect of EBL was effectively corrected by a powerful algorithm, PYRAMID according to fabrications results. The as-fabricated structures match well with their prototypes respectively in terms of geometry and resolution.

The influence of major factors involved in the experiments, dose coefficient, base dose, spot size, line spacing, developing time, developer concentration, and ultrasonic agitation was studied. All experimental factors except spot size appear to have significant influence in fabrication results upon geometry and resolution.

A statistics based methodology, Design of Experiment, was used to analyze the cross effect of factors and consolidate our conclusion. The response of experimental results was properly designed so that a statistical spreadsheet can be created accordingly. It is revealed from DOE that only base dose, developing time and developer ratio play an important role in fabrication process and so do their interactions according to ANOVA report. Finally, the optimization of the response was performed to seek optimum response based upon existing experimental data and 20 possible solutions are found. They were compared with existed experimental conditions in terms of achieving optimum response and a consistency between the optimized solutions and experiments was found.

References:

[1] K. Lu, M. Hiser and W. Wu, Powder Technology 192 (2009) 178.
[2] P. P. Lele and E. M. Furst, Langmuir 25 (2009) 8875.
[3] L. M. Goldenberg, Y. Gritsai, O. Sakhno, O. Kulikovska and J. Stumpe, Journal of Optics A: Pure and Applied Optics 12.
[4] R. J. Winfield, B. Bhuian, S. O'Brien and G. M. Crean, Applied Surface Science 253 (2007) 8086.
[5] J. H. Moon, S. Yang and S.-M. Yang, Applied Physics Letters 88 (2006).
[6] L. A. Woldering, A. P. Mosk, R. W. Tjerkstra and W. L. Vos, Journal of Applied Physics 105 (2009).
[7] D. Chanda, L. Abolghasemi and P. R. Herman, Optics Express 14 (2006) 8568.
[8] J. Ihlemann and D. Schafer, (SPIE, 2004) p. 455.
[9] P. Pal and K. Sato, Journal of Micromechanics and Microengineering 19 (2009).
[10] C. Wang, G. Jia, L. H. Taherabadi and M. J. Madou, Journal of Microelectromechanical Systems 14 (2005) 348.
[11] Y. Nanen, H. Yoshioka, M. Noborio, J. Suda and T. Kimoto, IEEE Transactions on Electron Devices 56 (2009) 2632.
[12] T. Chih-Chun, W. Chia-Hsin and L. Shen-Iuan, Solid-State Circuits, IEEE Journal of 37 (2002) 471.
[13] S.-C. Shen, M.-W. Wang and C.-J. Lee, Journal of Microelectromechanical Systems 18 (2009) 52.
[14] C. S. Premachandran, S. C. Chong, S. Liw and R. Nagarajan, IEEE Transactions on Advanced Packaging 32 (2009) 486.
[15] B. Morgan, C. M. Waits, J. Krizmanic and R. Ghodssi, Journal of Microelectromechanical Systems 13 (2004) 113.
[16] G. Cojoc, C. Liberale, P. Candeloro, F. Gentile, G. Das, F. De Angelis and E. Di Fabrizio, Microelectronic Engineering 87 876.
[17] S. J. Moon and S. S. Lee, Journal of Micromechanics and Microengineering 15 (2005) 903.
[18] Y. Xia and G. M. Whitesides, (Annual Reviews Inc, Palo Alto, CA, United States, 1998) p. 153.
[19] C. Marzolin, A. Terfort, J. Tien and G. M. Whitesides, Thin Solid Films 315 (1998) 9.
[20] S. Y. Chou, Nanoimprinting lithography, (1998).
[21] S. Y. Chou, Release surfaces, particularly for use in nanoimprinting lithography, (2001).
[22] S. Y. Chou, Fluid pressure imprint lithography, (2002).
[23] S. Y. Chou, Method and apparatus for high density nanostructures, (2003).
[24] P. R. Mirkin; Chad A., Hong; Seunghun Methods utilizing scanning probe microscope tips and products therefor or products thereby, (2003).
[25] M. Zhang, D. Bullen, S.-W. Chung, S. Hong, K. S. Ryu, Z. Fan, C. A. Mirkin and C. Liu, Nanotechnology 13 (2002) 212.

[26] S. Rozhok, R. Piner and C. A. Mirkin, Journal of Physical Chemistry B 107 (2003) 751.
[27] E. W. Becker, W. Bier, P. Bley, W. Ehrfeld, K. Schubert and D. Seidel, (AIChE, Orlando, FL, USA, 1982) p. 49.
[28] E. W. Becker, W. Ehrfeld, P. Hagmann, A. Maner and D. Muenchmeyer, Microelectronic Engineering 4 (1986) 35.
[29] C. K. Malek and V. Saile, Microelectronics Journal 35 (2004) 131.
[30] M. Eisner and J. Schwider, Optical Engineering 35 (1996) 2979.
[31] A. Maciossek, (Austin, TX, USA, 1996) p. 275.
[32] T. M. Bloomstein and D. J. Ehrlich, (Publ by IEEE, Nara, Jpn, 1991) p. 202.
[33] X.-Q. Sun, T. Masuzawa and M. Fujino, Sensors and Actuators, A: Physical 57 (1996) 159.
[34] T. Masaki, K. Kawata and T. Masuzawa, (Publ by IEEE, Napa Valley, CA, USA, 1990) p. 21.
[35] S. Zissi, A. Bertsch, J. Jézéquel, S. Corbel, D. Lougnot and J. André, Microsystem Technologies 2 (1996) 97.
[36] S.-Y. Lee, J. C. Jacob, C.-M. Chen, J. A. McMillan and N. C. MacDonald, Journal of Vacuum Science & Technology B: Microelectronics and Nanometer Structures 9 (1991) 3048.
[37] S.-Y. Lee and B. Liu, Journal of Vacuum Science and Technology B: Microelectronics and Nanometer Structures 14 (1996) 3874.
[38] S.-Y. Lee and B. D. Cook, IEEE Transactions on Semiconductor Manufacturing 11 (1998) 108.
[39] B. D. Cook and S.-Y. Lee, IEEE Transactions on Semiconductor Manufacturing 11 (1998) 117.
[40] S. Y. Lee and J. Laddha, (Elsevier, Jena, Germany, 2001) p. 303.
[41] S. Y. Lee and D. He, Microelectronic Engineering 69 (2003) 47.
[42] W. Chen and H. Ahmed, Applied Physics Letters 62 (1993) 1499.
[43] R. Murali, D. K. Brown, K. P. Martin and J. D. Meindl, Journal of Vacuum Science and Technology B: Microelectronics and Nanometer Structures 24 (2006) 2936.
[44] D. G. Hasko, S. Yasin and A. Mumtaz, Journal of Vacuum Science and Technology B: Microelectronics and Nanometer Structures 18 (2000) 3441.
[45] E. A. Dobisz, S. L. Brandow, R. Bass and J. Mitterender, Journal of Vacuum Science & Technology B: Microelectronics and Nanometer Structures 18 (2000) 107.
[46] S. Yasin, D. G. Hasko and H. Ahmed, Journal of Vacuum Science and Technology B: Microelectronics and Nanometer Structures 17 (1999) 3390.
[47] J. J. C. S. M. R. a. W. D. Westwood, in "Handbook of Plasma Processing Technology: Fundamentals, Etching, Deposition, and Surface Interactions" (William Andrew Publishing/Noyes, 1990) p. 200.
[48] D. Fairchild, Quality Engineering 10 (1998) 155.

Appendix. DOE design spreadsheet*

A	B	C	D	E	Ns	TR	H1	H2	H3	H4	H5	SH1	SH2	SH3	SH4	SH5	OH	MF	LnMF
1:3	50	25	10	1000	5	13.637	19.06	14.7	12.5	9.53	22.3	0.88	28.5	56.9	110	5.24	78	0.06781	-2.69109
1:3	50	55	8	1000	5	19.831	16.22	13.7	12.1	7.05	24.4	14.3	39.9	63.2	168	19.3	73.39	0.06515	-2.73111
1:3	50	10	8	1000	5	17.041	16.69	12.5	9.46	9.74	18.6	11	56	111	105	1.85	67.05	0.05977	-2.81727
1:3	50	25	8	1000	5	17.018	14.96	13	8.79	9.61	19.2	25.4	48.4	126	108	0.59	65.63	0.05524	-2.89599
1:3	100	10	6	500	5	18.153	34.32	18.4	12.4	12.44	14.3	205	2.46	57.8	57.8	32.5	91.85	0.05106	-2.97481
1:3	100	25	6	500	5	15.7	25.68	14.9	8.96	7.47	21.5	32.3	25.6	122	157	2.28	78.56	0.04631	-3.07243
1:3	100	25	8	500	5	16.109	27.39	14.9	7.36	8.14	15.7	54.6	26.3	160	141	18.9	73.41	0.04024	-3.21278
1:3	100	10	8	500	5	19.162	33.35	15.6	7.94	11.44	4.76	178	19.7	145	73.3	232	73.05	0.02953	-3.52238
1:5	100	25	10	1000	5	12.814	26.91	12	6.76	5.01	10.4	47.7	64	175	225	92.7	61.05	0.0212	-3.8538
1:5	100	10	8	1000	5	12.1	22.06	8.53	9.17	6.18	8.42	4.24	132	117	191	134	54.36	0.02093	-3.86668
1:5	100	25	8	1000	5	10.956	17.06	8.09	6.53	4.58	11	8.64	142	181	238	80.8	47.27	0.01684	-4.08391

1	1	1	1	1	5	9.9	24.	6.	8.	5.	1	18	1	1	2	8	55	0.01	-
:	0	0	0	0		351	29	1	5	0	1	.4	9	3	2	0.		535	4.17
5	0			0					6	3			3	1	4	6			663
1	1	2	1	2	5	9.2	26.	1	1	6.	3.	46	7	8	1	2	59.	0.01	-
:	0	5	0	5		291	81	1.	0.	4	6	.4	1.	2.	8	6	48	423	4.25
3	0							6	9	8	9		2	1	3	6			23
1	5	2	8	1	5	10.	7.6	6.	4.	3.	1	15	1	2	2	3.	40.	0.01	-
:	0	5		0		15	2	5	2	6	8.	3	8	4	6	1	39	195	4.42
5				0				9	8	8	2		0	7	6	7			74
1	5	1	6	5	5	8.0	26.	8.	5.	2.	6.	38	1	2	3	1	50.	0.00	-
:	0	0		0		357	24	8	8	3	8	.9	2	0	1	7	12	947	4.65
5	0							4		6	8		5	2	1	2			949
1	5	1	8	5	5	8.0	27.	9	4.	4.	6.	55	1	2	2	1	51.	0.00	-
:	0	0		0		105	46		9	0	2	.7	2	2	5	8	69	945	4.66
5	0								7	2	4		1	6	5	9			124
1	5	2	6	5	5	7.2	24.	8.	4.	3.	5.	19	1	2	2	2	46.	0.00	-
:	0	5		0		529	38	0	6	3	7	.2	4	3	7	0	12	824	4.79
5	0							5		4	5		3	7	8	3			825
1	5	1	6	1	5	7.4	7.6	5.	4.	2.	1	15	1	2	3	5	33.	0.00	-
:	0	0		0		88	3	9	4	6	2.	3	9	4	0	4.	28	789	4.84
5				0				2	7	3	6		8	1	2	3			156
1	1	2	8	2	5	7.0	15.	6.	3.	4.	6.	18	1	2	2	1	36.	0.00	-
:	0	5		5		499	65	4	5	2	6	.9	8	7	4	7	57	784	4.84
3	0								6	7	9		5	0	7	7			799
1	5	2	8	5	5	6.6	20.	6.	3.	2.	6.	0.	1	2	2	1	40.	0.00	-
:	0	5		0		805	15	9	8	9	2	02	7	6	9	9	13	733	4.91
5	0							7	7	4			0	0	1	0			586
1	5	5	6	1	5	6.3	10.	4.	4.	3.	8.	84	2	2	2	1	32.	0.00	-
:	0			0		005	79	4	4	8	8	.8	4	4	6	2	39	661	5.01
5				0				3	3	8	6		2	2	0	4			964
1	5	2	1	5	5	6.1	24.	6.	4.	2.	5.	20	1	2	3	2	42.	0.00	-
:	0	5	0	0		503	54	0	2	5	0	.6	9	4	0	2	32	618	5.08
5	0							1	6		1		6	8	6	5			627
1	5	1	8	1	5	6.1	9.7	4.	3.	3.	7.	10	2	2	2	1	29.	0.00	-
:	0	0		0		251		5	9	8	4	6	3	5	6	5	45	599	5.11
5				0				6	2		7		8	9	2	7			76
1	5	2	6	1	4	7.8	7.2	5.	4.		1	16	2	2	4	6	28.	0.00	-
:	0	5		0		629		2	1		1.	4	1	5	0	5.	52	573	5.16
5				0				8	6		9		7	1	0	9			165
1	5	2	1	1	5	7.9	45.	9.	6.	4.	5.	63	1	1	2	2	70.	0.00	-
:	0	5	0	0		932	16	1	4	1	4	3	1	8	5	1	29	571	5.16
5	0			0				5	2		6		8	4	3	1			52
1	1	2	6	2	5	5.1	9.8	3.	2.	2.	6.	10	2	2	3	1	25.	0.00	-
:	0	5		5		328		8	9	4	1	4	6	9	0	9	14	444	5.41
3	0							2	4	5	3		2	1	8	2			816
1	1	1	6	2	5	5.0	9.6	5.	2.	2.	5.	10	2	3	3	2	24.	0.00	-

:	0	0		5		083	7	0	6	0	3	7	2	0	2	1	91	43	5.44
3	0							8	9	9	8		3	0	1	4			806
1	5	2	1	1	3	7.9	11	5.			1	81	2	4	4	6	28.	0.00	-
:	0	5	0	0		991		7			1.		0	0	0	7.	52	417	5.48
5				0				6			8		3	0	0	9			047
1	5	1	1	1	3	8.8	0	0	6.	4.	1	40	4	1	2	5	23.	0.00	-
:	0	0	0	0		035			0	7	2.	0	0	9	3	3	56	413	5.48
5				0					9	5	7		0	3	3				955
1	5	2	1	2	5	4.1	13.	4.	2.	2.	4.	38	2	3	3	2	27.	0.00	-
:	0	5	0	5		375	78	0	5	3	3	.7	5	0	1	4	17	359	5.62
5	0							6	8	6	9		4	3	1	4			836
1	5	2	1	5	5	4.4	6.8	4.	2.	2.	5.	17	2	3	3	2	20.	0.00	-
:	0	5	0	0		886	8	5	0	0	3	2	3	2	2	1	91	354	5.64
3								5	9	9			9	1	1	6			402
1	5	1	6	2	5	4.1	10.	3.	2.	2.	3.	82	2	2	3	2	23.	0.00	-
:	0	0		5		64	9	5	8	5	4	.8	7	9	0	7	35	34	5.68
5	0							6	7	8	4		0	3	3	4			358
1	5	2	6	2	5	3.4	10.	2.	3.	1.	2.	92	3	2	3	3	20.	0.00	-
:	0	5		5		624	39	6	2	8	4	.4	0	8	2	0	63	264	5.93
5	0							8	5	7	4		0	1	9	8			578
1	5	2	8	5	5	3.8	3.7	2.	1.	1.	3.	26	3	3	3	2	12.	0.00	-
:	0	5		0		771	2	5	1	7	7	5	0	5	3	6	86	254	5.97
3									3	6	5		6	6	3	4			409
1	5	2	8	2	5	3.0	16.	2.	2.	1.	2.	9.	2	2	3	2	26.	0.00	-
:	0	5		5		35	98	9	9	3	8	12	9	9	4	9	94	245	6.01
5	0									1	5		2	2	9	4			054
1	1	1	8	5	5	3.3	5.1	1.	2.	1.	4.	22	3	3	3	2	14.	0.00	-
:	0	0		0		089		8	1	7	1	2	3	2	3	5	9	227	6.08
5	0							4	1		5		0	0	5	1			818
1	5	1	8	5	5	3.3	3.9	2.	2.	1.	3.	25	3	3	3	2	13.	0.00	-
:	0	0		0		32	6	2	2	8	4	7	1	1	3	7	7	223	6.10
3								1	1	4	8		6	6	0	3			493
1	5	2	8	2	5	3.1	3.9	1.	2.	1.	3.	25	3	3	3	2	12.	0.00	-
:	0	5		5		137	6	6	5	1	6	7	3	0	5	6	95	205	6.19
3								4	4	9	2		7	5	4	8			154
1	1	2	1	5	5	2.9	6.2	2.	1.	1.	3.	18	3	3	3	2	14.	0.00	-
:	0	5	0	0		946	7	1	5	6	0	9	2	3	3	8	69	204	6.19
5	0							2	8	8	4		0	9	6	8			673
1	5	5	6	1	2	11.	52.				5.	10	4	4	4	2	58.	0.00	-
:	0			0		568	96				1	86	0	0	0	2	07	184	6.29
5	0			0							1		0	0	0	2			528
1	5	2	6	1	2	10.	49.				6.	86	4	4	4	1	55.	0.00	-
:	0	5		0		347	43				1	6	0	0	0	9	57	183	6.30
5	0			0							4		0	0	0	2			198
1	5	2	8	1	2	8.4	46.				3.	70	4	4	4	2	50.	0.00	-
:	0	5		0		881	49				9	2	0	0	0	5	45	157	6.45

5	0			0								6		0	0	0	7			503
1	5	1	8	2	5	3.0							40	4	4	4	4	0	0.00	-
:	0	0		5		555							0	0	0	0	0		153	6.48
3														0	0	0	0			396
1	5	1	6	1	2	9.0	55.					6.	12	4	4	4	1	61.	0.00	-
:	0	0		0		672	2					0	39	0	0	0	9	26	138	6.58
5	0			0								6		0	0	0	4			764
1	5	1	8	1	2	7.8	49.					4.	88	4	4	4	2	54.	0.00	-
:	0	0		0		557	78					4	7	0	0	0	4	2	135	6.60
5	0			0								2		0	0	0	3			85
1	5	5	6	5	5	1.8	1.3					1.	34	4	4	4	3	3.3	0.00	-
:	0			0		007	7					9	7	0	0	0	2	3	096	6.94
5												6		0	0	0	5			686
1	1	2	8	5	2	3.2	5.9					4.	19	4	4	4	2	10.	0.00	-
:	0	5		0		249	7					9	7	0	0	0	2	94	079	7.13
5	0											7		0	0	0	6			726
1	1	2	6	5	2	3.1	5.7					3.	20	4	4	4	2	9.1	0.00	-
:	0	5		0		093	8					3	2	0	0	0	7	1	074	7.20
5	0											3		0	0	0	8			85
1	5	2	1	2	5	1.1	0.8	0.	0.	0.		0.	36	3	3	3	3	3.4	0.00	-
:	0	5	0	5		562	7	5	6	7		7	6	8	7	7	7	2	062	7.38
3								1		2		2		0	6	2	2			621
1	5	2	1	5	2	1.7	3.7					2.	26	4	4	4	3	6.1	0.00	-
:	0	5	0	0		979	1					4	5	0	0	0	0	9	041	7.80
5												8		0	0	0	7			971
1	5	1	8	5	2	1.7	2.4					3.	30	4	4	4	2	5.6	0.00	-
:	0	0		0		73	3					2	9	0	0	0	8	7	04	7.83
5												4		0	0	0	1			337
1	5	2	8	5	2	1.7	3.4					2.	27	4	4	4	3	5.8	0.00	-
:	0	5		0		611	5					3	4	0	0	0	1	2	039	7.83
5												7		0	0	0	1			737
1	5	5	6	5	1	3.3						7.	40	4	4	4	1	7.6	0.00	-
:	0			0		931						6	0	0	0	0	5	5	039	7.85
5	0											5		0	0	0	3			651
1	5	2	6	5	2	1.0	3.1					3.	28	4	4	4	2	6.5	0.00	-
:	0	5		0		988	9					3	3	0	0	0	7	1	025	8.29
5												2		0	0	0	8			559
1	5	1	8	2	1	2.3						3.	40	4	4	4	2	3.5	0.00	-
:	0	0		5		326						5	0	0	0	0	7	1	025	8.29
5	0											1		0	0	0	2			717
1	5	1	6	5	1	1.6							40	4	4	4	4	0	0.00	-
:	0	0		0		434							0	0	0	0	0		016	8.71
5														0	0	0	0			357
1	1	1	8	2	1	1.1						1.	40	4	4	4	3	1.6	0.00	-
:	0	0		5		945						6	0	0	0	0	3	1	012	9.00
5	0											1		0	0	0	8			122

1	1	2	8	2	1	0.8	2.	40	4	4	4	3	2.0	9.2	-
:	0	5		5		841	0	0	0	0	0	2	1	E-	9.29
5	0						1		0	0	0	4		05	46
1	1	2	6	2	1	0.8	4.	40	4	4	4	2	4.4	9.1	-
:	0	5		5		366	4	0	0	0	0	4	9	E-	9.30
5	0						9		0	0	0	1		05	567
1	5	2	1	2	1	0.7	5.	40	4	4	4	2	5.4	8.4	-
:	0	5	0	5		626	4	0	0	0	0	1	4	E-	9.38
5							4		0	0	0	2		05	264
1	5	1	1	1	0	5.7		40	4	4	4	4	0	0	
:	0	0	0	0		75		0	0	0	0	0			
5	0			0					0	0	0	0			
1	1	1	6	1	0			40	4	4	4	4	0	0	
:	0	0		0				0	0	0	0	0			
3	0			0					0	0	0	0			
1	1	2	6	1	0			40	4	4	4	4	0	0	
:	0	5		0				0	0	0	0	0			
3	0			0					0	0	0	0			
1	1	2	8	1	0			40	4	4	4	4	0	0	
:	0	5		0				0	0	0	0	0			
3	0			0					0	0	0	0			
1	1	1	8	1	0			40	4	4	4	4	0	0	
:	0	0		0				0	0	0	0	0			
3	0			0					0	0	0	0			
1	1	5	6	1	0			40	4	4	4	4	0	0	
:	0			0				0	0	0	0	0			
3	0			0					0	0	0	0			
1	5	1	6	2	0			40	4	4	4	4	0	0	
:	0	0		5				0	0	0	0	0			
3	0								0	0	0	0			
1	1	5	6	2	0			40	4	4	4	4	0	0	
:	0			5				0	0	0	0	0			
5	0								0	0	0	0			
1	1	5	8	2	0			40	4	4	4	4	0	0	
:	0			5				0	0	0	0	0			
5	0								0	0	0	0			
1	5	5	6	2	0			40	4	4	4	4	0	0	
:	0			5				0	0	0	0	0			
5									0	0	0	0			
1	5	1	6	2	0			40	4	4	4	4	0	0	
:	0	0		5				0	0	0	0	0			
5									0	0	0	0			
1	5	1	6	2	0			40	4	4	4	4	0	0	
:	0	0		5				0	0	0	0	0			
3									0	0	0	0			
1	5	5	8	2	0			40	4	4	4	4	0	0	

:	0			5			0	0	0	0	0							
5								0	0	0	0							
1	5	1	8	2	0		40	4	4	4	4	0	0					
:	0	0		5			0	0	0	0	0							
5								0	0	0	0							
1	5	2	6	2	0		40	4	4	4	4	0	0					
:	0	5		5			0	0	0	0	0							
5								0	0	0	0							
1	1	1	6	2	0		40	4	4	4	4	0	0					
:	0	0		5			0	0	0	0	0							
5	0							0	0	0	0							
1	5	5	6	1			40	4	4	4	4	0	0					
:	0			0			0	0	0	0	0							
3				0				0	0	0	0							
1	5	1	6	5			40	4	4	4	4	0	0					
:	0	0		0			0	0	0	0	0							
3								0	0	0	0							
1	5	1	6	1			40	4	4	4	4	0	0					
:	0	0		0			0	0	0	0	0							
3				0				0	0	0	0							
1	5	2	6	2			40	4	4	4	4	0	0					
:	0	5		5			0	0	0	0	0							
3								0	0	0	0							
1	5	2	6	5			40	4	4	4	4	0	0					
:	0	5		0			0	0	0	0	0							
3								0	0	0	0							
1	5	2	6	1			40	4	4	4	4	0	0					
:	0	5		0			0	0	0	0	0							
3				0				0	0	0	0							
1	1	1	8	2			40	4	4	4	4	0	0					
:	0	0		5			0	0	0	0	0							
3	0							0	0	0	0							
1	5	2	8	2			40	4	4	4	4	0	0					
:	0	5		5			0	0	0	0	0							
5								0	0	0	0							

*A--Developing ratio, B--Developing time, C--Line spacing, D--spot size, E--base dose, Ns--number of steps counted in the pattern, TR--the RMS roughness of the pattern, Height i--The height of the i^{th} individual steps, such as H1 represents the height of 1^{st} step, H2 2^{nd}, H3 3^{rd} etc, Shi--the square of difference between 20 and i^{th} step hight, such as

SH1 represents the square of difference between 20 and 1st step height, OH--Overall height of the pattern, MF--Multiply factor, LnMF--Natural logarithm of MF.